Memoirs of the Faculty of Engineering, Nagoya University
Vol. 29, No. 2. (1977)

A STUDY ON Al-Mn ALLOYS SOLIDIFIED BY RAPID COOLING

SEIKI NISHI and TETSUYUKI IKEDA

Department of Metallurgy

(received October 31, 1977)

CONTENTS

I Introduction 124
II Experimental Procedures 125
1. Specimens 125
2. The apparatus used for thermal analysis 126
3. Micro-Vickers hardness measurment and tensile test 127
4. Measurement of lattice parameters by x-ray 128
5. Analyses of x-ray diffraction patterns and EPMA line-scanning profiles ... 128
III Experimental Results and Discussion 128
1. Cooling curves and the solidifying conditions 128
2. Alloy structures solidified by rapid cooling 131
2. 1. The structure changes of Al-Mn alloys influenced by an increase of thickness distance in ingots 131
2. 1. 1. Al-1.0 wt%Mn alloy (a hypo-eutectic alloy) 131
2. 1. 2. Al-2.0 wt%Mn alloy (an eutectic alloy) 131
2. 1. 3. Al-2.9 wt%Mn alloy (a hyper-eutectic alloy) 133
2. 2. The consideration of structures solidified by rapid cooling based on x-ray diffraction results 134
2. 2. 1. The change in lattice parameters of Al-Mn alloys 134
2. 2. 2. Structures solidified by rapid cooling and crystallized compound phases 135
3. The change in mechanical properties with the change of solidified structures 136
3. 1. Micro-Vickers hardness 136
3. 2. Tensile strength 138
3. 3. Elongation 139
4. The structure distribution in ingots solidified by rapid cooling and the conditions for formation of these structures 141
4. 1. The relation between solidified structures and, the changes in micro-Vickers hardness and lattice parameters with an increase in thickness distance 141
4. 2. The structure distribution diagram 142
4. 3. The relation between the change in lattice parameters and the structure distribution diagram based on the micro-Vickers hardness change 144
4. 4. The condition diagram for formation of solidified structures 145

5. The solidification mode of a super-saturated solid solution and the super-saturated solid solubility phenomenon 146
5. 1. The solidification model and the analysis on results of thermal analysis 146
5. 2. The solidification mode of super-saturated solid solutions 148
5. 3. The thickening rate of solid cells (local solidification process) 150
5. 4. The theoretical interpretation of the super-saturated solid solubility phenomenon 151
6. The phase decomposition of a completely super-saturated solid solution 153
6. 1. Isothermal heating 153
6. 2. Precipitated phases and precipitation process 155
7. The analysis on the precipitation - decomposition process in a completely super-saturated solid solution 157
7. 1. The analysis method of the precipitation - decomposition process 157
7. 2. The kinetic consideration on the precipitation process 160
7. 3. The decomposition process of a completely super-saturated solid solution 161
7. 4. The activation energy for the precipitation - decomposition 162
Ⅳ Summary 162
References 163

I Introduction

In order to improve mechanical properties of aluminium alloys, plastic working, refinement of macrostructure and heat treatment have been used.[1] In the field of foundry engineering, especially the grain refinement[2~6] and the segregation phenomenon[7~11] have been studied so long time. However, the improvement of mechanical properties based on the refinement of macrostructure is considered to be limited. Therefore, to improve mechanical properties more, we tried to refine microstructure,[12~15] get a super-saturated solid solution[16~20] and then age-harden its super-saturated solid solution.[17, 21] For this study, solidification methods based on rapid cooling[22~26] were adapted as the most suitable method and such study has not been done systematically over a wide range of composition on any alloys yet.

Usually Al-Mn alloys are used as wrought products[27~29] and have a tendency that easily a super-saturated solid solution is obtained by relatively small cooling rates.[16, 30, 31] As the purpose of this study was to improve properties of casting products being in a super-saturated state, we used Al-Mn alloys obtained by a rapid solidification method and the behaviors of solute manganese atoms in such state were investigated. Namely, (1) the change of solidified structures by solidification rates and structure distribution in cast products of Al-1 ~ 5 wt%Mn alloys,[32, 33] (2) the change in mechanical properties by the change of solidified structures,[20] (3) the consideration on the super-saturated solid solution phenomenon by making to clear the solidification mode of a super-saturated solid solution[34] and (4) the change of characteristics in a super-saturated Al-3 wt%Mn solid solution by heat treatment and its precipitation - decomposition process[35, 36] were the subjects of this study.

II Experimental Procedures

1. Specimens

Al-Mn alloys used were made by an Al-Mn master alloy containing 13.0 wt%Mn and commercial purity aluminium (99.8 wt%) and cast in ingots of 350～450 g. They had manganese contents previously determined. Specimens for thermal analysis were 15～50 g weight which were cut from these ingots. These alloys were cast in a water-cooled copper chill mold (Fig. 1 (a)), in which three thermo-couples

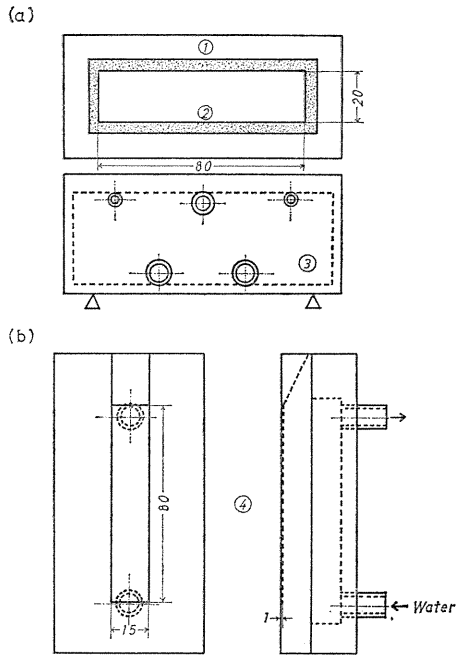

Fig. 1. Molds used for rapid solidification.
(a) for unidirectional solidification,
(b) for bi-directional solidification
① Graphite frame, ② Asbestos,
③ Water-cooled copper chill,
④ Water-cooled copper mold

were set, by the natural drop technique after holding for 5 minutes at 850℃ and then the dropped melt solidified unidirectionally. Specimens obtained by rapid solidification were 20 mm in width, 8 mm in length and up to 7 mm in thickness. In order to make a completely super-saturated solid solution of an Al-3 wt%Mn alloy which is used for heat treatment test, a water-cooled copper mold shown in Fig. 1 (b) was used and rapid solidification was made under always the same melting condition. The super-saturated solid solution was 15 mm in width, 50 mm in length and 1 mm in thickness. Heat treatment was carried out in a salt bath consisting of $NaNO_3$ and KNO_3 of pre-determined temperatures for 10 min to 60 hr. The manganese contents of all the specimens used for this study are shown in Table 1.

As these alloys made by commercial grade metals, iron and silicon are contained in these alloys as impurities.

Table 1. Chemical composition of the specimens.

specimen \ element		Mn (wt%)	Si (wt%)	Fe (wt%)
As Quenching	1.0%Mn	1.02	0.07	0.04
	2.0%Mn	2.03	0.06	0.05
	2.9%Mn	2.86	0.07	0.04
	3.6%Mn	3.61	0.08	0.04
	4.4%Mn	4.36	0.08	0.04
Heat Treatment	3 %Mn	3.09	0.09	0.08

2. The apparatus used for thermal analysis

Fig. 2 is the schematic diagram of the apparatus used for rapid solidification by the natural drop technique.[26] By an elema furnace an Al-Mn alloy piece was

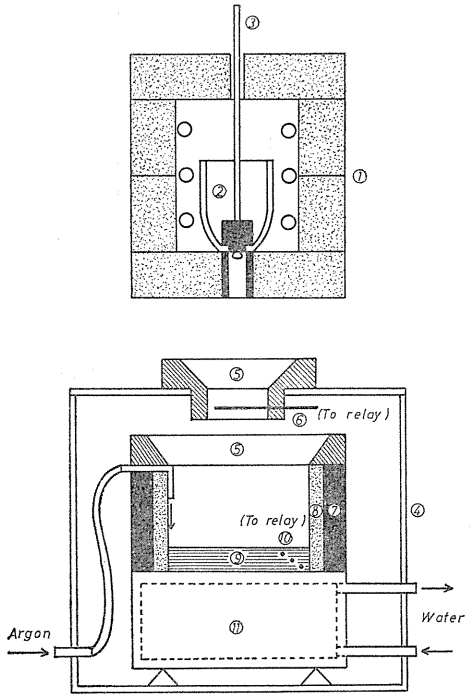

Fig. 2. Schematic diagram of the apparatus for rapid cooling.
① Furnace, ② Crucible, ③ Stopper, ④ Mold, ⑤ Sprue, ⑥ Trigger, ⑦ Graphite frame, ⑧ Asbestos, ⑨ Specimen, ⑩ A. C. thermocouple, ⑪ Water-cooled copper chill

melted in a graphite crucible which had a hole at bottom closed by a graphite stopper. The mold was set at 300 mm under the furnace bottom. This mold has side walls insulated by asbestos plates inserted in contact with the walls and a water-cooled copper chill on which Ar gas was blown. Alumel-chromel thermocouples with about 0.32 mm were used. The hot junction was coated with alumina. Three junctions were set about 1.5, 3.0 and 4.5 mm from a chilled surface in the mold, before the melt was poured. Fig. 3 is the thermal analysis circuit used for

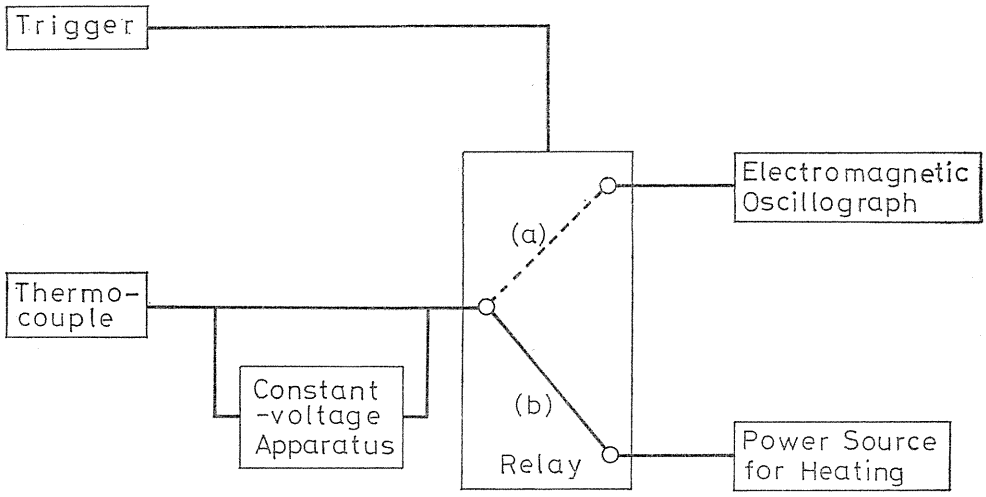

Fig. 3. Thermal analysis circuit of rapid cooling. (a) after the trigger is short-circuited by the molten metal, and (b) before short-circuited

measurment of the rapid solidification process. Each thermocouple was pre-heated at about 800℃ by an electric current of 5～6A. When by lifting the stopper, the molten alloy fell down through a hole at bottom of the crucible, a trigger which was set between the furnace and the mold was short-circuited by the molten alloy. Then, the relay circuit was switched from (b) to (a). Electric current by which the thermocouples were pre-heated is turned off and the solidification process of the melt is recorded with an electromagnetic oscillograph.

3. Micro-Vickers hardness measurement and tensile test

The specimens for thermal analysis were cut perpendicular to a chilled surface and the cut surface was finished by electropolishing, along thickness distance (distance from a chilled surface) micro-Vickers (with 100 g load) hardness was measured at interval 0.25 or 0.5 mm points from a chilled surface. On the remaining specimens, plates with 1 mm thickness for tensile test were cut parallel to a chilled surface and at intervals of 1 mm. After the test pieces were finished to 7 mm wide at the parallel part and with 250 mm in gage length, and were polished with No. 1000 emery paper. Tensile test was made with a strain rate of 1.3×10^{-3} mm/mm·sec. After the specimens heat-treated were electropolished on a section parallel to a chilled surface at solidification, micro-Vickers hardness was measured on the section.

4. Measurement of lattice parameters by x-ray

Concerning to specimens solidified by rapid cooling and heat-treated (on polished surfaces parallel to a chilled surface and at each 1 mm or 0.5 mm interval) which were measured the hardness, lattice parameters of Al-Mn solid solutions were determined by diffractometer with Cu-Kα radiation filtered with nickel. Only for resolved doublets in diffraction lines of higher angle than a (200) plane, lattice parameters were calculated from wave lengthes for Cu-Kα_1 radiation (1.54051 Å) and for Cu-Kα_2 (1.54433 Å). Those values were plotted by Nelson-Riley function and a value extrapolated to a Bragg angle of 90° gave exact lattice parameters.[37] For the correction of angle, 99.9 wt% silicon powder was used as the standard sample.

5. Analyses of x-ray diffraction patterns and EPMA line-scanning profiles

Diffraction patterns of crystallized compounds in typical structures solidified by rapid cooling and precipitated phases in the typical structures after heat treatment were obtained by using Cu-Kα radiation filtered with nickel. Furthermore, in order to find the species of crystallized compounds in the solidified structures, the line-scanning analyses on manganese, iron and silicon were carried out with EPMA. Ternary compounds precipitated were confirm by the line-scanning analyses on manganese and silicon repeatedly.

III Experimental Results and Discussion

1. Cooling curves and the solidifying conditions[32]

In order to measure the conditions for rapid solidification in this study, three hot junctions of thermocouples were set in the ingot at three points, that is, at

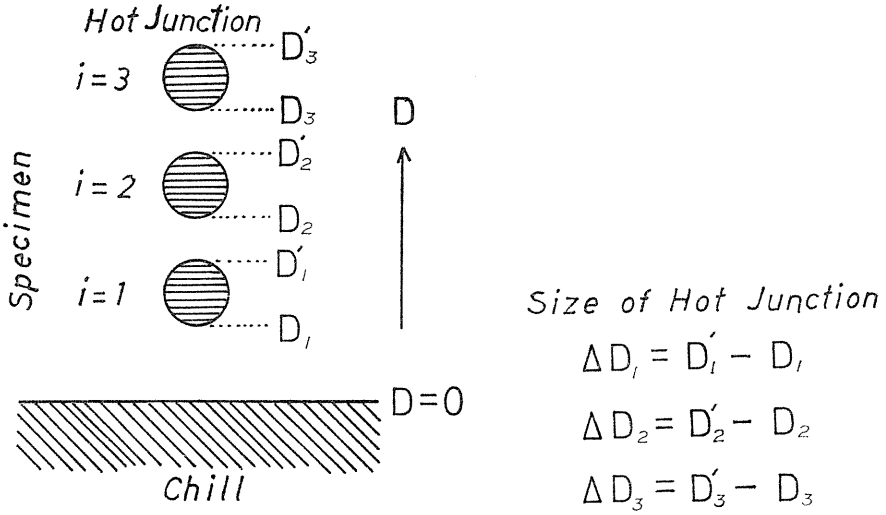

Fig. 4. Size and thickness distance of the hot junctions.

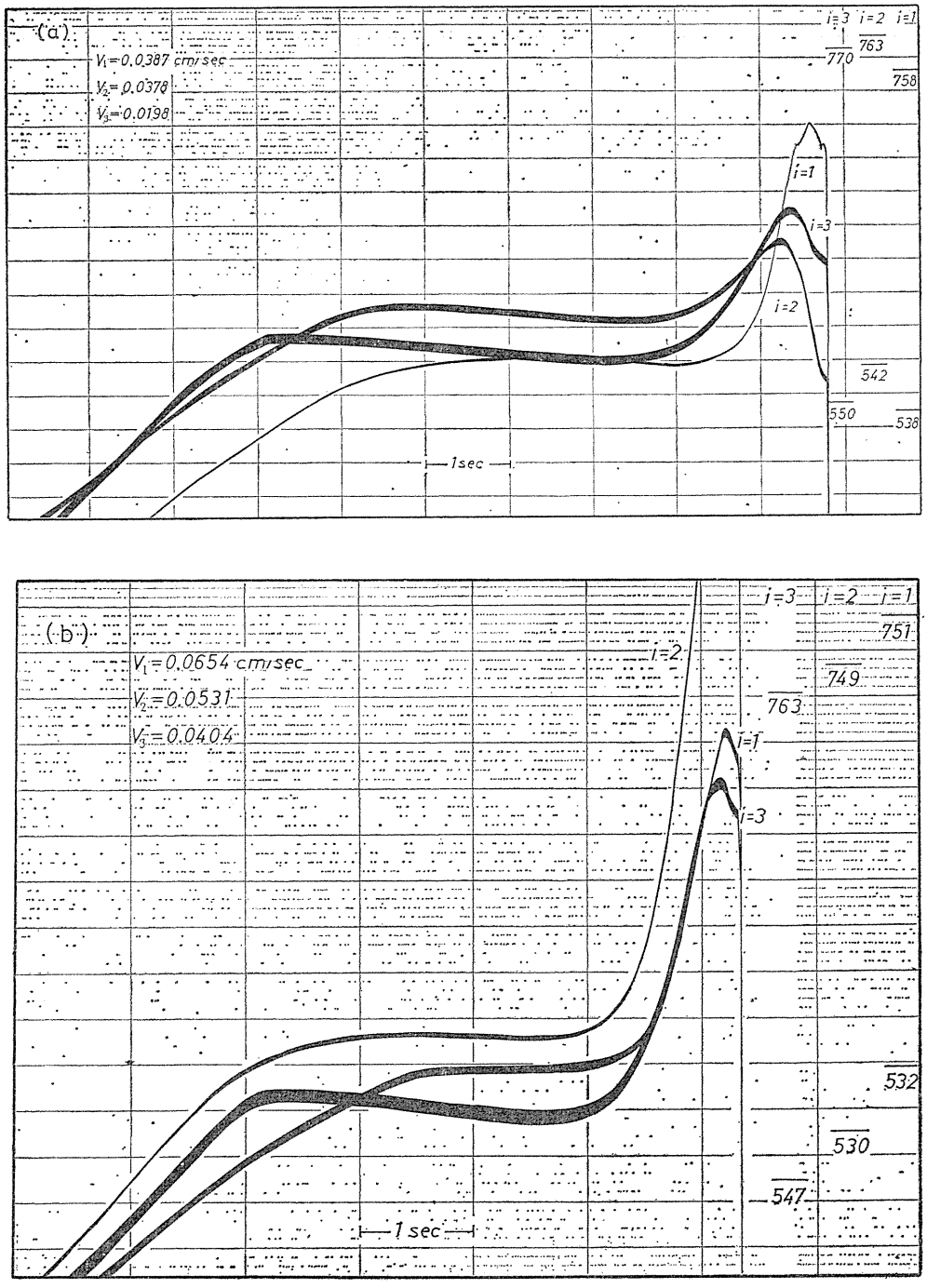

Photo. 1. Typical cooling curves of the rapid solidification for Al-2.9 wt%Mn alloy.

(a) $\overline{V}_i$=0.0383 cm/sec

(b) $\overline{V}_i$=0.0593 cm/sec

about 1.5 mm (D_1), 3.0 mm (D_2) and 4.5 mm (D_3) from the chilled surface, respectively, as shown in Fig. 4 and thermal analysis was made with those. Two typical cooling curves recorded by this method are shown in Photo. 1. The cooling curve (a) in Photo. 1 is of the case that the incompletely super-saturated solid solution of an Al-2.9 wt%Mn alloy was formed and (b) is of the completely super-saturated solid solution of an Al-2.9 wt%Mn alloy. The cooling curves of $i=1$, $i=2$ and $i=3$ are those recorded the local solidification process at about 1.5 mm, 3.0 mm and 4.5 mm in thickness distance from the chilled surface, respectively. The temperature scale on each cooling curve is written on the right side in Photo. 1 with constant voltage pulses. Fig. 5 are cooling curves schematically drawn. The arrest time (i. e. local solidification time) shown on a cooling curve is obtained by the following equation:

$$\Delta t_i = t'_i - t_i \quad (i=1\sim3) \tag{1}$$

where Δt_i is local solidification time, t_i is the beginning time of local solidification and t'_i is the ending time of that. Therefore, as shown in Fig. 6, the moving rate

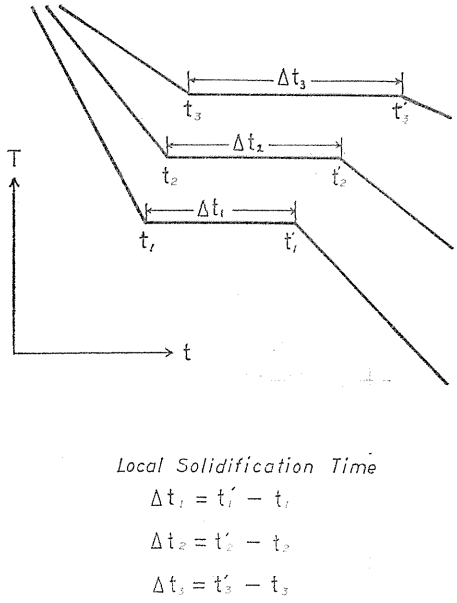

Fig. 5. Local solidification time, starting time of local solidification and the ending time of cooling curves.

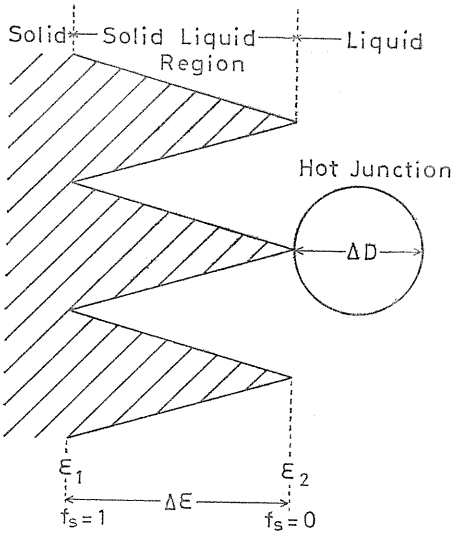

Fig. 6. Relation between the position of a hot junction for liquid-solid region and solidification rate.

of the liquid-solid region V_i ($d(\Delta\varepsilon)/dt$), that is, the rate at which the liquid-solid region passes a hot junction with ΔD diameter, is expressed as Eq. (2):

$$V_i = \Delta D_i / \Delta t_i \quad (i=1\sim3) \tag{2}$$

where the diameter of a hot junction ΔD_i is determined by x-ray radiograph and Δt_i is the arrest time obtained from a cooling curve. After this V_i is taken as

solidification rate, then the average value of solidification rates measured with three thermocouples is taken as the average solidification rate.

2. Alloy structures solidified by rapid cooling[20,32,33]

2. 1. The structure changes of Al-Mn alloys influenced by an increase of thickness distance in ingots

2. 1. 1. Al-1.0 wt%Mn alloy (a hypo-eutectic alloy)

Microstructures of the Al-1.0 wt%Mn alloy solidified by rapid cooling are a uniform solid solution of a single α-phase as shown in Photo. 2 (a) and (b), and show the cellular structure (morphology of network).[16,38] Therefore, in the range of solidification rates of this study, only cell size changed from 10μ to 60μ with an increase in thickness distance and other changes were not found in these structures.

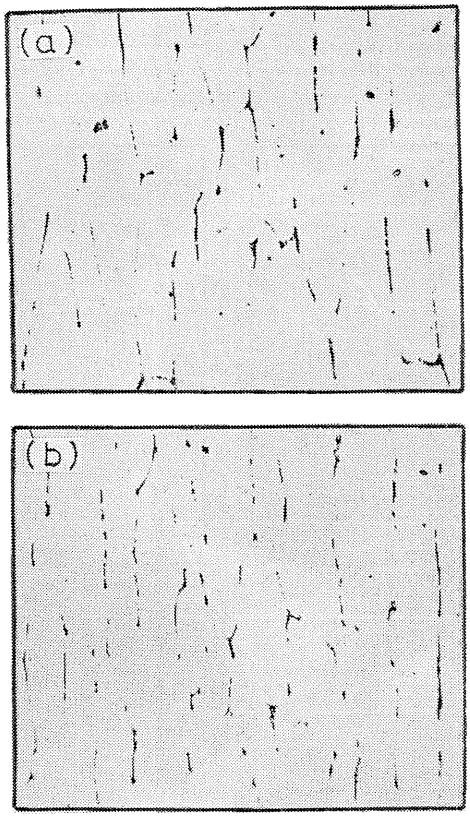

Photo. 2. Microstructures of Al-1.0 wt%Mn alloy. (X250)
(a) V_i=0.0136 cm/sec, (b) V_i=0.0394 cm/sec

2. 1. 2. Al-2.0 wt%Mn alloy (an eutectic alloy)

About the specimens of an Al-2.0 wt%Mn alloy (an alloy of the eutectic composition) solidified by rapid cooling, microstructures changed by an increase in

thickness distances as shown in Photo. 3. Then, this change corresponds to the change of microstructures by a decrease in solidification rates. The structure (a) is a completely super-saturated solid solution (single α-phase) which is distributed

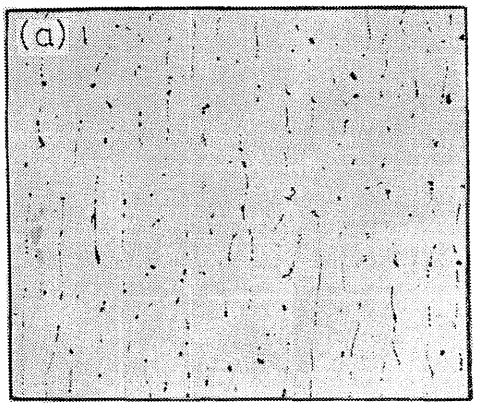

completely super-saturated solid solution (α)

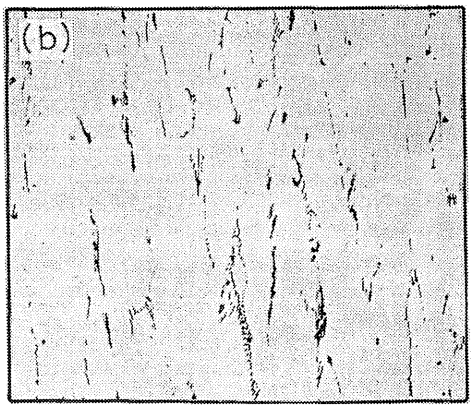

incompletely super-saturated solid solution (hypo-eutectic)

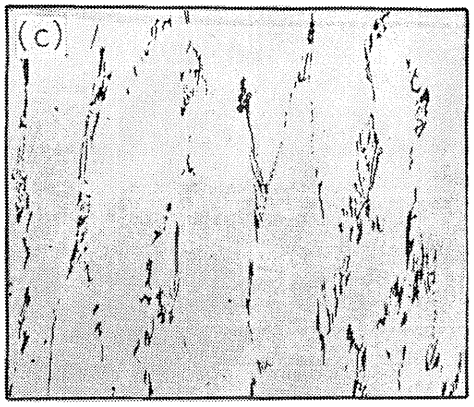

incompletely super-saturated solid solution (hypo-eutectic)

structure formed by displacement of the eutectic point (hypo-eutectic)

Photo. 3. Change of microstructures with thickness distance for Al-2.0 wt%Mn alloy. (X 250)

at a chilled portion (the vicinity of a surface where a specimen is in contact with a chill). Then, the structure (b) is the incompletely super-saturated solid solution of a hypo-eutectic type (the mixed structure consisting of a super-saturated solid solution and secondary phases). The structure (c) is that at a place where thickness distance increased further, and is the incompletely super-saturated solid solution of a hypo-eutectic type. As in the structure of this case many compound phases are found, the amount of super-saturated solid solubility may be less compared with the structure (b). The structure (d) is a hypo-eutectic structure corresponding to a structure formed by displacement of the eutectic point. In the conditions for solidification in this study, an eutectic structure corresponding to an equilibrium structure could not be found within 8 mm in thickness distance.

2. 1. 3. Al-2.9 wt%Mn alloy (a hyper-eutectic alloy)

About the specimens of an Al-2.9 wt%Mn alloy solidified by rapid cooling, the change of microstructures with an increase in thickness distances is shown in Photo. 4. With an increase in thickness distances, the structures change from (a) to (f)

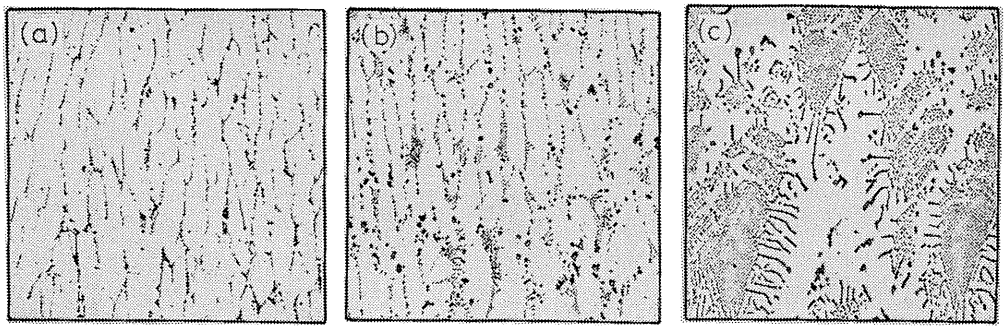

completely super-saturated solid solution

incompletely super-saturated solid solution of a hypo-eutectic type

incompletely super-saturated solid solution of a cellular eutectic type

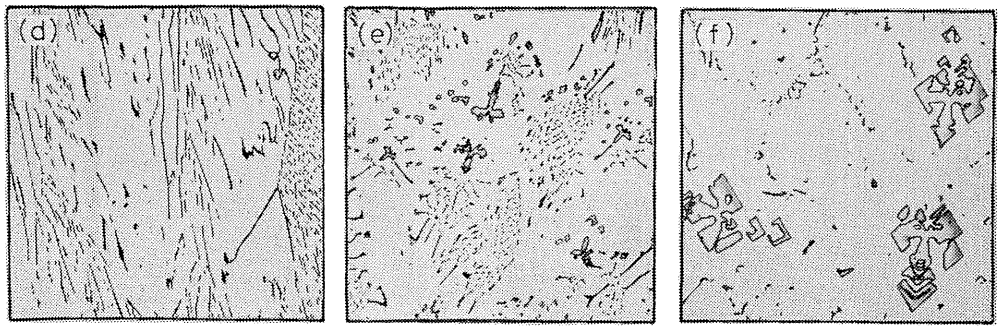

incompletely super-saturated solid solution of an acicular eutectic type

primary compound + eutectic

primary compound + solid solution

Photo. 4. Change of microstructures with thickness distance for Al-2.9 wt%Mn alloy. (X 200)

according to the distance from the chilled surface and the structure (a) is a completely super-saturated solid solution of a single α-phase which distributes at a chilled portion. In this structure, all phases found at cell boundaries are Al-Fe compounds. The structure (b) is an incompletely super-saturated solid solution of a hypo-eutectic type. That of (c) is an incompletely super-saturated solid solution of a cellular eutectic type. The structure (d) is an incompletely super-saturated solid solution with acicular eutectic compounds, shown as a cellular type. The structure (e) is a primary compounds - eutectic structure which is formed by displacement of the eutectic point and the structure (f) is a primary compounds - α structure which is an equilibrium structure.

2. 2. The consideration of structures solidified by rapid cooling based on x-ray diffraction results

2. 2. 1. The change in lattice parameters of Al-Mn alloys

The changes of lattice parameters on Al-Mn solid solution matrix, influenced by an increase in solidification rate, are shown in Fig. 7. For example, for an Al-2.9 wt%Mn alloy, the lattice parameters of an equilibrium structure (primary compounds and α-phase) and a structure formed by displacement of the eutectic point

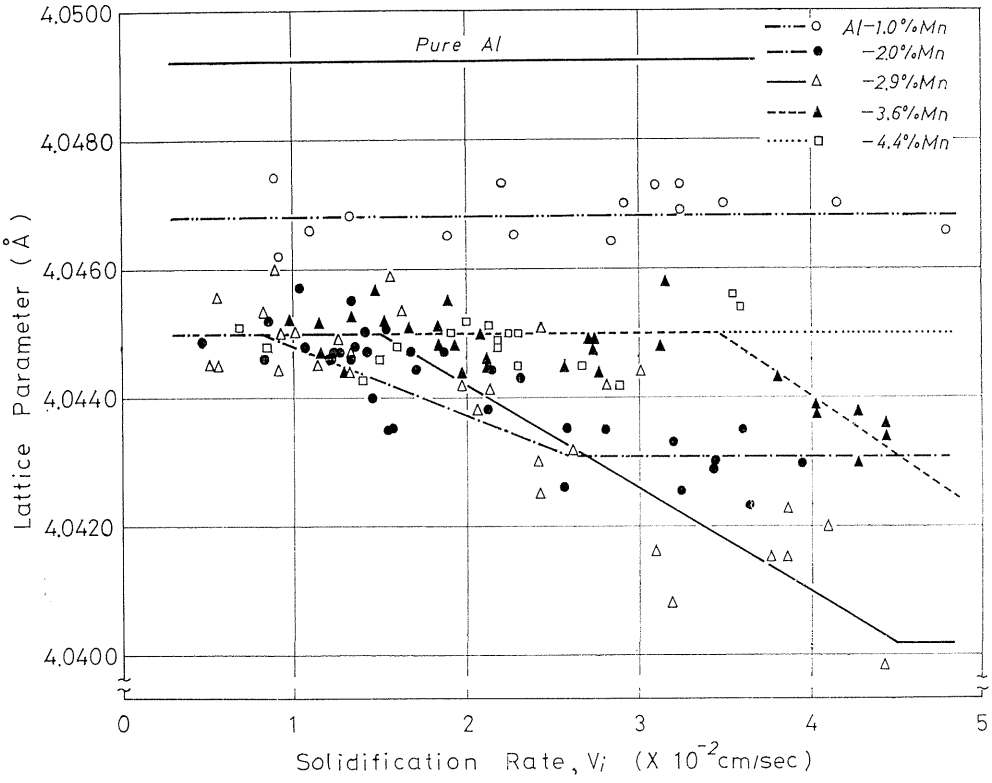

Fig. 7. Change in the lattice parameter with solidification rate for Al-Mn alloys.

(primary compounds and eutectic) were equally a fixed value of 4.045Å, which is obtained at solidification rates below 1.5×10^{-2} cm/sec. Therefore, perhaps, the Al-Mn solid solutions may contain the concentration[39] of the maximum equilibrium solubility 1.4 wt%Mn.[40] At a range of solidification rate (1.5×10^{-2} to 4.5×10^{-2} cm/sec), the super-saturated solid solubility of manganese increases, an incompletely super-saturated solid solution appears and lattice parameter decreases. That is, at solidification rates above 4.5×10^{-2} cm/sec, the completely super-saturated solid solution of a single α-phase is obtained and the lattice parameter changes to a fixed value of 4.040Å. Concerning to the change of structures of Al-2.0 wt%Mn and Al-3.6 wt%Mn alloys, the change of the lattice parameter is similar to that of an Al-2.9 wt%Mn alloy. Therefore, at solidification rates below 0.8×10^{-2} cm/sec

for an Al-2.0 wt%Mn alloy and below 3.5×10^{-2} cm/sec for an Al-3.6 wt%Mn alloy, the lattice parameters were a fixed value of 4.045Å. When solidification rate increases above these values, the lattice parameters are less than 4.045Å. However, for an Al-2.0 wt%Mn alloy, as solidification rate becomes above 2.6×10^{-2} cm/sec, the lattice parameter showed a fixed value of 4.043Å. The lattice parameters of an Al-1.0 wt%Mn alloy (below the composition of the maximum equilibrium solubility limit) were a fixed value of 4.0465Å over all ranges of solidification rate used in this study ($0.5\times10^{-2}\sim7.0\times10^{-2}$ cm/sec). Moreover, for an Al-4.4 wt%Mn alloy, the lattice parameter is a fixed value of 4.045Å. However, in this case the structure changed from primary compounds - α-phase to primary compounds - eutectic.

2. 2. 2. Structures solidified by rapid cooling and crystallized compound phases

In Fig. 8, we summarize the relations between solidified structures and the change of crystallized compound phases, brought by change of solidification rates,

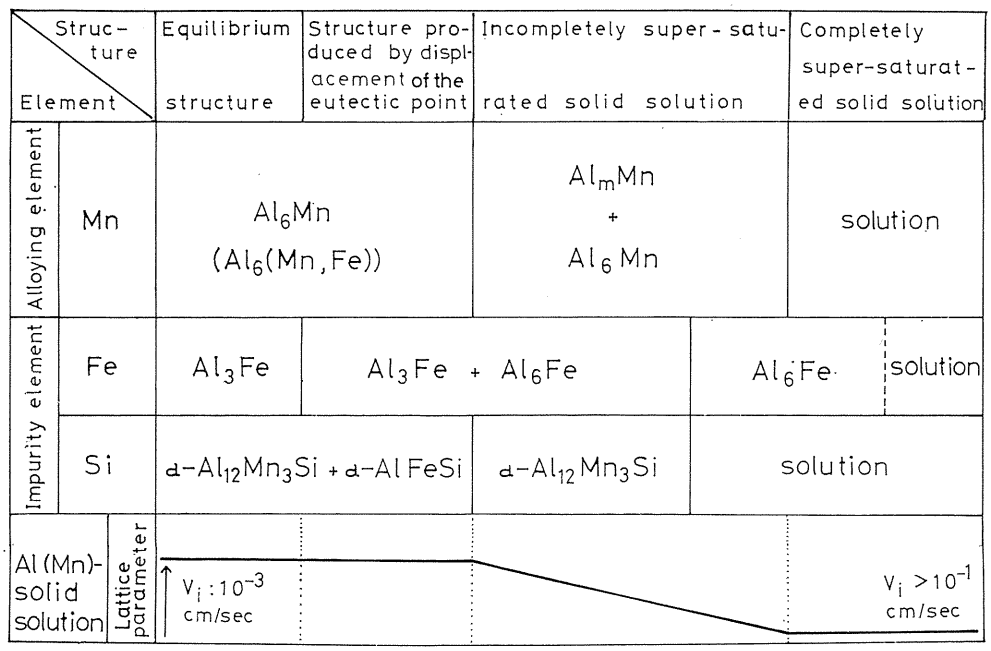

Fig. 8. Schematic figure illustrating relation between crystallized phases and solidified structures for rapidly solidified Al-Mn alloys.

by analyzing the x-ray diffraction patterns and the EPMA line-scanning profiles. Crystallized Al-Mn compound phases found in an incompletely super-saturated solid solution structure are the metastable intermediate phase Al_mMn (simple cubic system, $a_0=12.727$Å)[33] and the equiliburium phase Al_6Mn (orthorhombic system, $a_0=6.50$Å, $b_0=7.55$Å, $c_0=8.87$Å).[41] In a structure formed by displacement of the eutectic point and an equiliburium structure, the Al_6Mn and the primary compound $Al_6(Mn, Fe)$[42] are identified. Iron, an impurity element, crystallizes at cell bound-

aries as the metastable phase Al_6Fe (orthorhombic system, $a_0=6.49$Å, $b_0=7.44$Å, $c_0=8.79$Å).[43] Even if structure is a completely super-saturated solid solution or an incompletely super-saturated solid solution of a hypo-eutectic type, it crystallizes also as Al_6Fe compounds. In an incompletely super-saturated solid solution with a cellular eutectic type structure and a structure formed by displacement of the eutectic point, the Al_6Fe and the equiliburium phase Al_3Fe (monoclinic system, $a_0=15.49$Å, $b_0=8.08$Å, $c_0=12.48$Å, $\beta=107°43'$)[44] coexist.

Also, silicon crystallizes as ternary compounds, that is, in an incompletely super-saturated solid solution of a cellular eutectic type, α-$Al_{12}Mn_3Si$ (b. c. c. system, $a_0=12.65\pm0.15$Å)[42] crystallized and in a structure formed by displacement of the eutectic point and an equiliburium structure, the α-$Al_{12}Mn_3Si$ and α-Al-Fe-Si (b. c. c. system, $a_0=12.548$Å)[42] crystallized. Hypo-eutectic alloys (2.0 to 1.4 wt%Mn) crystallize the intermetallic compounds of manganese and iron systems and alloys of manganese compositions below the maximum equiliburium solubility, for example an Al-1.0 wt%Mn alloy, crystallize the compound phases of a iron system.

3. *The change in mechanical properties with the change of solidified structures*[20]

3. 1. *Micro-Vickers hardness*

Fig. 9 and Fig. 10 show the changes in micro-Vickers hardness, with an increase

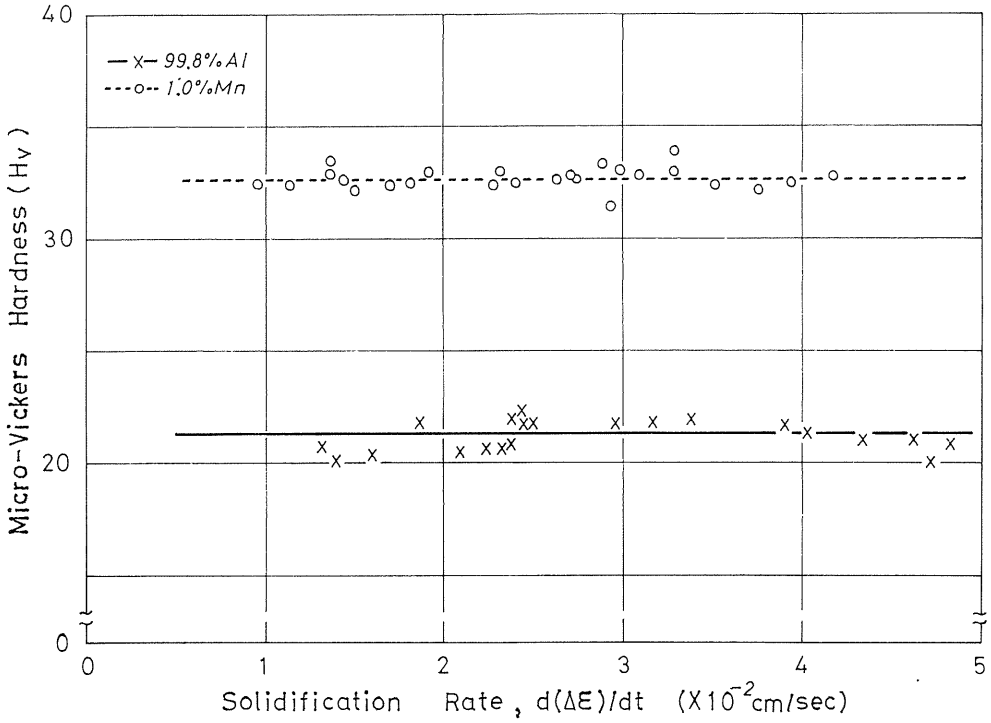

Fig. 9. Change in micro-Vickers hardness with solidification rate for 99.8 wt% Al and Al-1.0 wt%Mn alloy.

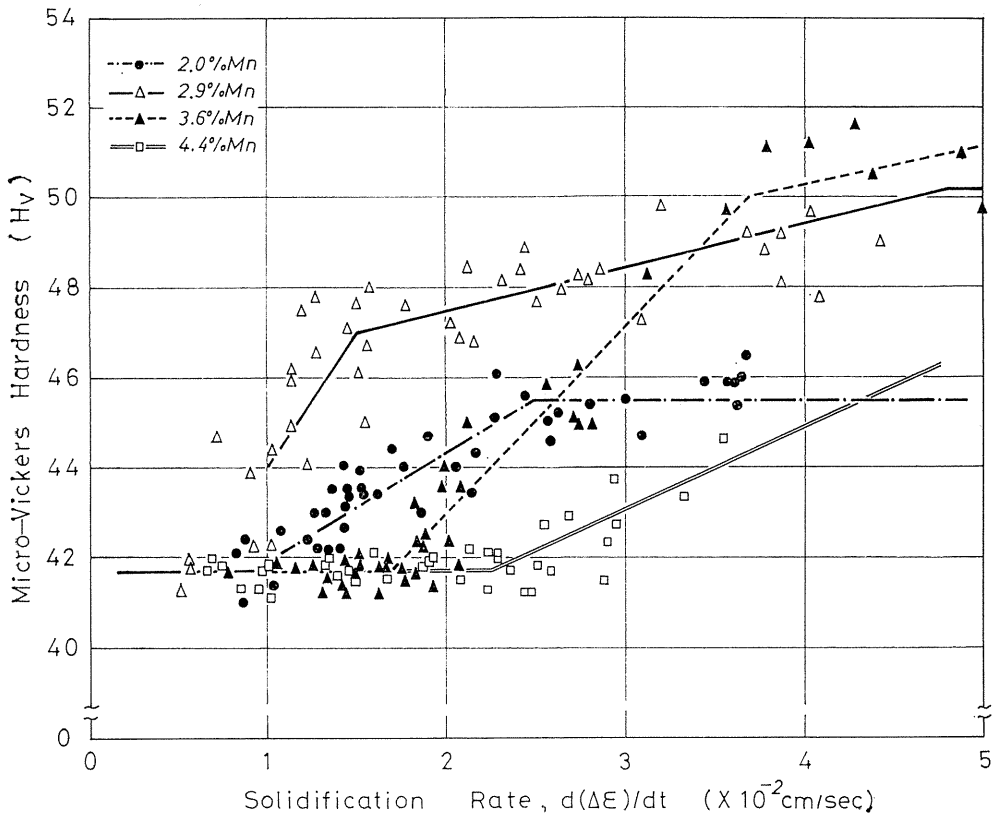

Fig. 10. Change in micro-Vickers hardness with solidification rate for Al-Mn alloys.

in solidification rates, of pure aluminium (99.8 wt%) and Al-Mn alloys containing various amount of manganese. Even if the solidification rate increases, pure aluminium and an Al-1.0 wt%Mn alloy show 21.3 and 32.6 in micro-Vickers hardness respectively and the refinement hardening of subgrains[45,46] was not recognized. Next, in case of slow solidification rates (below 0.6×10^{-2} for an Al-2.9 wt%Mn, 1.7×10^{-2} for an Al-3.6 wt%Mn alloy and 2.2×10^{-2} cm/sec for an Al-4.4 wt%Mn alloy, respectively) followed by a primary compounds - α structure, a fixed hardness value 41.7 H_V was obtained. When solidification rates increase above 0.6×10^{-2}, 1.7×10^{-2} and 2.2×10^{-2} cm/sec, structures become those formed by displacement of the eutectic point (that is, those structures are consisted of primary compounds and eutectic) and the hardness (H_V) increased severally from 41.7 to 47.0, from 41.7 to 50.0 and over 41.7 according as manganese contents of the alloys described previously increases. This increase is brought by the dispersion hardening of eutectic compounds. When the solidification rate increases further (that is, solidification rates become above 0.9×10^{-2} cm/sec for an Al-2.0 wt%Mn alloy, 1.5×10^{-2} cm/sec for an Al-2.9 wt%Mn alloy and 3.7×10^{-2} cm/sec for an Al-3.6 wt%Mn alloy, respectively), in every Al-Mn alloy the super-saturated solid solubility takes place and incompletely super-saturated solid solutions of an eutectic structure or a hypo-

eutectic structure are obtained. The hardness H_V increases still from 41.7 to 45.5, from 47.0 to 50.2 and over 50.0 by the solid solution hardening of manganese. At solidification rates above 2.5×10^{-2} cm/sec for an Al-2.0 wt%Mn alloy and above 4.9×10^{-2} cm/sec for an Al-2.9 wt%Mn alloy, a completely super-saturated solid solution of a single α-phase is obtained and the hardness H_V indicates fixed values of 45.5 and 50.2.

3. 2. Tensile strength

Fig. 11 shows the change in ultimate tensile strength with an increase in solidification rates for pure aluminium and the alloys of various compositions. The change in ultimate tensile strength of the hyper-eutectic alloys, that is, Al-2.9 wt%Mn, Al-3.6 wt%Mn and Al-4.4 wt%Mn alloys shows the same tendency as

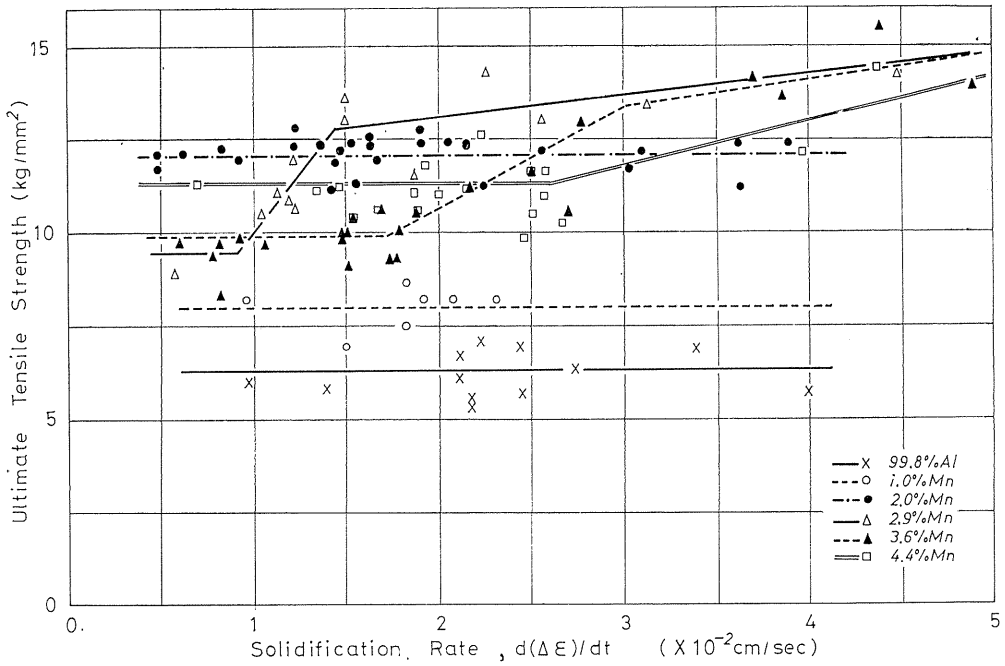

Fig. 11. Change in ultimate tensile strength with solidification rate for Al-Mn alloys.

micro-Vickers hardness. However, in the region of solidification rates that a primary compounds - α structure corresponding to equiliburium is obtained, since the amount of primary compounds increases with an increase in manganese compositions, ultimate tensile strength increases as 9.5, 9.9 and 11.3 kg/mm^2 gradually. Futhermore, the solidification rate increases and in regions of solidification rates that a primary compounds - eutectic structure and an incompletely super-saturated solid solution appear, ultimate tensile strength values σ_B for an Al-2.9 wt%Mn alloy increase from 9.5 to 12.8 kg/mm^2 and from 12.8 to 14.8 kg/mm^2 respectively, because of the dispersion strengthening of eutectic compounds and the solid solution strengthening. Also those for an Al-3.6 wt%Mn alloy increase linearly from 9.9 to

13.4 kg/mm² and over 13.4 kg/mm², respectively and those for an Al-4.4 wt%Mn alloy increase linearly over 11.3 kg/mm². Ultimate tensile strength values for pure aluminium and an Al-1.0 wt%Mn alloy are fixed values of 6.3 and 8.0 kg/mm² respectively. Though structures of an Al-2.0 wt%Mn alloy changed from the structure formed by displacement of the eutectic point of hypo-eutectic to that of the completely super-saturated solid solution of a single α-phase, the ultimate tensile strength σ_B was 12.1 kg/mm² in any case.

3. 3. Elongation

Fig. 12 shows the change in elongation with an increase in solidification rates for pure aluminium and the alloys of respective manganese contents. In pure aluminium, an Al-1.0 wt%Mn alloy and the super-saturated solid solution of an Al-2.0 wt%Mn alloy, that is, those structures were a single α-phase, elongation increases

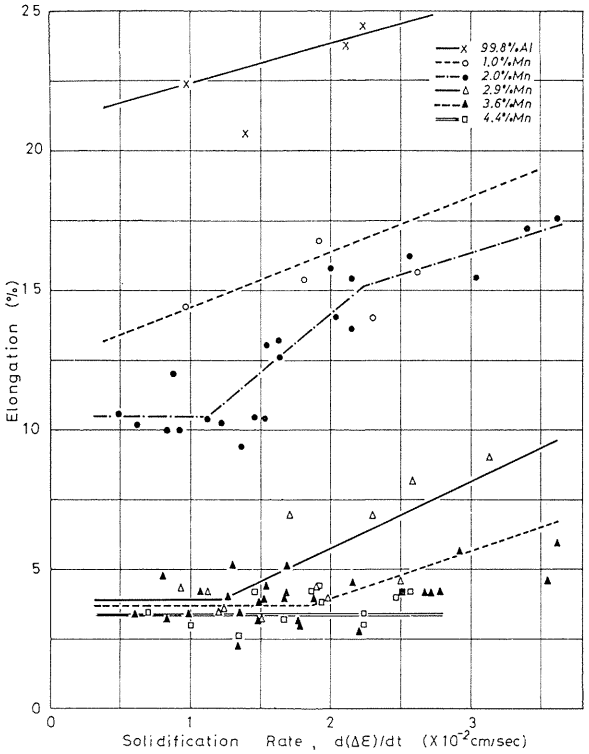

Fig. 12. Change in elongation with solidification rate for Al-Mn alloys.

linearly by the effect of the refinement of cellular grains with an increase in solidification rates.[47] However, in a primary compounds - α structure and a primary compounds - eutectic structure of the hyper-eutectic alloys in which rod like primary compounds set in array, elongation was fixed values until the solidification rates attain to several fixed values. Since the amount of primary compounds increases as the manganese compositions of the alloys increases, these elongation values decrease slightly. In case solidification rates increased further, an increase

of elongation values was observed since the amount of primary compounds decreased markedly.[3)]

From results described above, tendencys of change in mechanical properties (that is, ultimate tensile strength σ_B, micro-Vickers hardness H_V and elongation δ) on the material solidified by rapid cooling with an increase in solidification rates

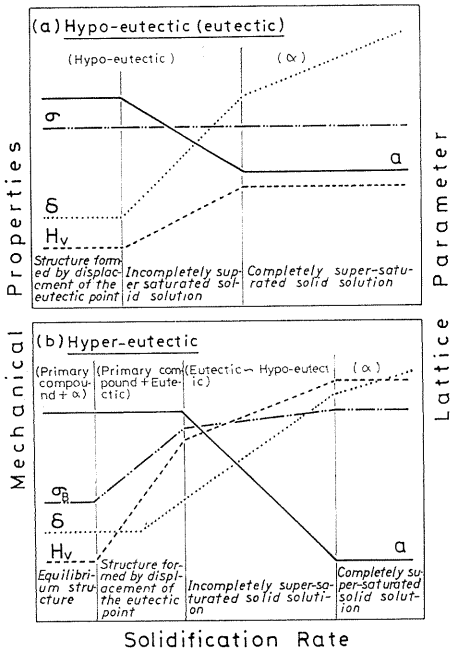

Fig. 13. Schematic figure illustrating changes in mechanical properties and lattice parameter with solidification rate or the change of solidified structures for Al-Mn alloys.

are illustrated by Fig. 13 in which lattice parameter is added to indicate the solid solution state of manganese. The (a) is the case of the alloys containing a hypo-eutectic composition and the (b) is that of the alloys containing a hyper-eutectic composition. In the (a), there is not so much change in ultimate tensile strength, but in an incompletely super-saturated solid solution the hardness rises. When structure changes to the completely super-saturated solid solution of a single α-phase, ductility becomes better. On the one hand, when the alloy is of a hyper-eutectic composition which has a structure formed by displacement of the eutectic point, the dispersion strengthening by eutectic compounds is obtained and in case solidification rates increase further and super-saturated solid solubility arises, mechanical properties are improved by the solid solution strengthening further. It can be concluded that especially, when the alloys having more manganese compositions had completely super-saturated solid solutions containing more manganese compositions, their thoughness was improved fairly.

4. The structure distribution in ingots solidified by rapid cooling and the conditions for formation of these structures[20, 32, 33]

4. 1. The relation between solidified structures and, the changes in micro-Vickers hardness and lattice parameters with an increase in thickness distance

For the change of the structure of an Al-2.9 wt%Mn alloy described in **III**-*2*, the changes in micro-Vickers hardness and lattice parameters with thickness distance at two solidification rates are shown in Fig. 14 (a), (b) about the fast case and the slow case, that is, in these case each average solidification rate is 1.58×10^{-2} cm/sec and 0.56×10^{-2} cm/sec, respectively. In the fast case, a completely

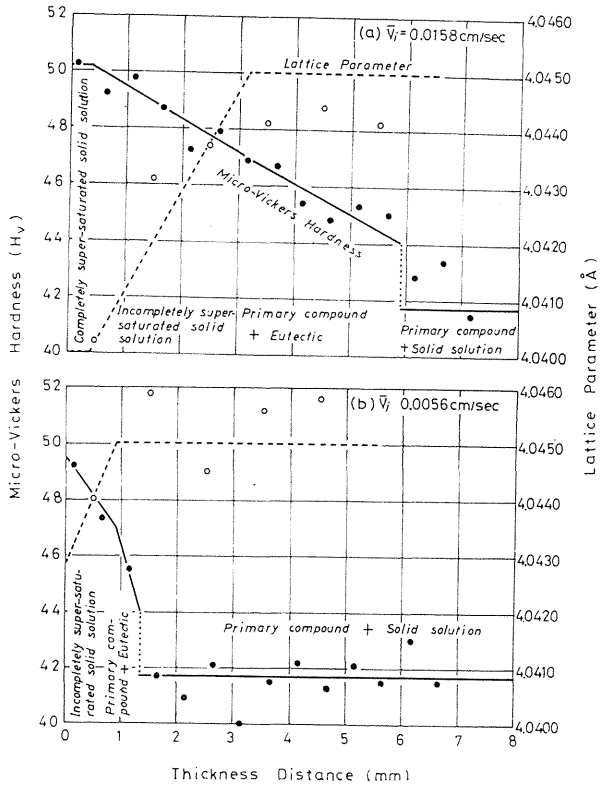

Fig. 14. Micro-Vickers hardness and lattice parameter changes with thickness distance.

super-saturated solid solution is obtained at the neighbourhood of a chilled surface less than 0.5 mm thickness distance and an incompletely super-saturated solid solution distributed over a range from 0.5 mm to 3.0 mm thickness distance. Furthermore, when thickness distance increases, at thickness distances above 3.0 mm a primary compounds - eutectic structure which is formed by displacement of the eutectic point appears and at thickness distances above 6.0 mm a primary compounds - α structure corresponding to an equilibrium structure.

In the slow case, a completely super-saturated solid solution is not found even at a chilled surface therefore and even less than 1.0 mm thickness distance, the structure becomes an incompletely super-saturated solid solution. At thickness distances from 1.0 to 1.2 mm, structure changes to a primary compounds - eutectic structure in the same manner as the specimen of the fast case and at thickness distances over 1.2 mm the structure changes to a primary compounds - α structure.

4. 2. The structure distribution diagram

About the specimens of an Al-2.9 wt%Mn alloy obtained by different average solidification rates, the change in micro-Vickers hardness with thickness distance is investigated, and inflection points were found on hardness curves and Fig. 15 shows the relation among average solidification rates, thickness distances and structures. Namely, this is the structure distribution diagram which expresses the correspondence between inflection points on the hardness curves and the discontinuity of

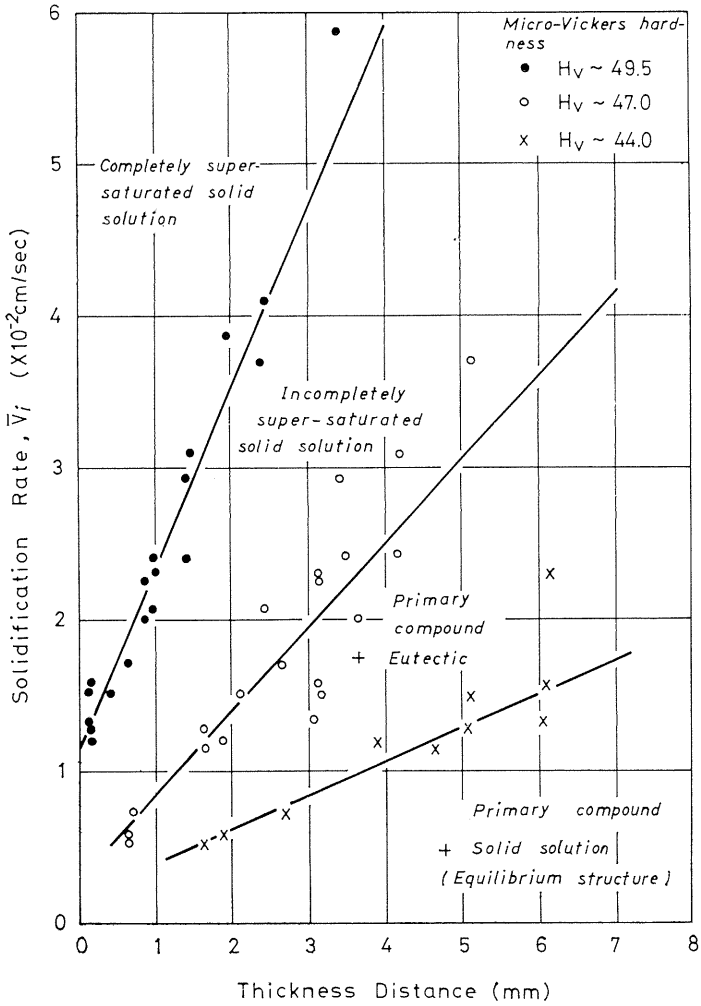

Fig. 15. The structure distribution diagram for Al-2.9 wt%Mn alloy.

structural distribution. While in a high solidification rate, the completely super-saturated solid solution of a single α-phase distributes on a wide range, in a low solidification rate a super-saturated solid solution is not found even at the neighbourhood of a chilled surface and a primary compounds - α structure corresponding to equilibrium distributes in a wide range.

On the basis of the structure diagrams as Fig. 15 for Al-1.0～4.4 wt%Mn alloys, the manganese contents (up to 5 wt%Mn) v. s. thickness distance diagrams for specified average solidification rates are shown in Fig. 16 (a) and (b). This shows the effect of manganese contents on the structural distribution. In the slow case of solidification rates, structures of equilibrium and displacement of the eutec-

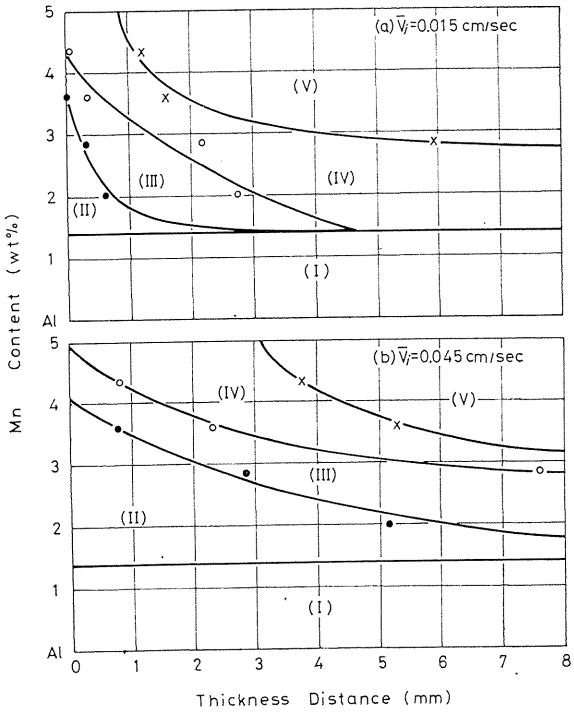

Fig. 16. The manganese content v. s. thickness distance structure diagram for Al-Mn alloys.
region I : solid solution,
region II : completely super-saturated solid solution,
region III : incompletely super-saturated solid solution,
region IV : structure formed by displacement of the eutectic point,
region V : equilibrium structure

tic point distribute widely up to low manganese compositions and small thickness distances. On the other hand in the case of high solidification rates, the region of a completely super-saturated solid solution expands up to samples of high manganese compositions and large thickness distances domain and, for example, at a solidification rate of 4.5×10^{-2} cm/sec, it became evident that the completely super-saturated solid solution of an Al-2.0 wt%Mn alloy is formed until about 6 mm thickness

distance of the sample. When it is necessary to get an aimed structure in given manganese composition alloys or low solidification rates, the structure diagrams will give standards about thickness of ingots and solidification conditions.

4. 3. The relation between the change in lattice parameters and the structure distribution diagram based on the micro-Vickers hardness change

The values of lattice parameter determined on the specimens of an Al-2.9 wt%Mn alloy solidified in some average solidification rates $\overline{V}_i$ were classified into next ranges, that is, less than 4.042Å, (namely this corresponds to solid solubility of about 2.9 wt% manganese),[40] from 4.042Å to 4.044Å (namely solid solubility from 2.9 wt% to 1.4 wt% manganese)[40] and above 4.044Å (namely solid solubility of about 1.4 wt% manganese),[40] and Fig. 17 is a diagram which shows the relation between lattice parameters and the structure diagram shown by Fig. 15 at the same solidification conditions each other. Both boundary lines determined by lattice parameter groupings and hardness ranges almost conincide as the figure. Since the boundary line between a primary compounds - eutectic structure and a primary compounds - α one was not obtained by this experiments, it is shown with a broken line. This is due to that the manganese contents of a solid solution in eutectic and that of a α-phase are similarly 1.4 wt% manganese (the composition of the maximum equilibrium solubility limit).

Also the relation between the structure distribution obtained from the change of lattice parameters and that obtained from hardness measurement was manifested.

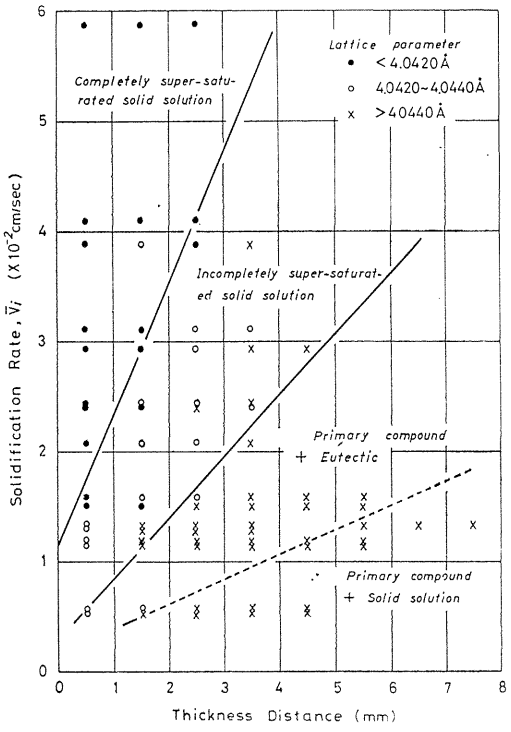

Fig. 17. Relation between lattice parameter and the structure distribution diagram based on micro-Vickers hardness.

4. 4. The condition diagram for formation of solidified structures

The mechanical properties of the super-saturated Al-Mn alloy solid solution obtained by rapid cooling is improved considerably as described in **III**-*3*. Then it is necessary to clear the minimum conditions of solidification rates which is required to get these structures. In micro-Vickers hardness change curves (in Fig. 10), with an increase in solidification rates, for the alloys containing each amount of manganese, there exist solidification rates at which the discontinuity in the hardness change takes place, and on the basis of these values, the conditions to form solidified structures of the alloys containing up to 5 wt% manganese are illustrated by Fig. 18. Region I shows the conditions for formation of a uniform solid solution

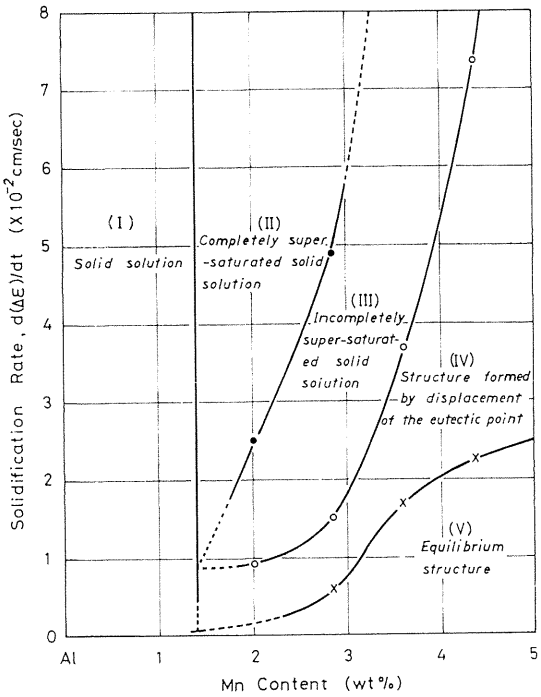

Fig. 18. The condition to form some solidified structures of rapidly solidified Al-Mn alloys.

(solid solubility below 1.4 wt%Mn),[36] region II for a completely super-saturated solid solution (super-saturated solid solubility above 1.4 wt% manganese), region III for an incompletely super-saturated solid solution (the added manganese does not dissolve completely in solid but is soluble more than 1.4 wt% manganese), region IV for a structure formed by displacement of the eutectic point and region V for an equilibrium structure. Exactly speaking, the region V should be expressed as the region of an equilibrium structure at the time when solidification has just finished. Therefore, this diagram expresses that in order to form an incompletely super-saturated solid solution and a completely super-saturated solid solution in an Al-2.0 wt%Mn alloy, solidification rates over 0.9×10^{-2} cm/sec and 2.5×10^{-2} cm/sec are required, respectively.

5. The solidification mode of a super-saturated solid solution and the super-saturated solid solubility phenomenon[32, 34]

5. 1. The solidification model and the analysis on results of thermal analysis

Regarding the structures of a completely super-saturated solid solution, an incompletely super-saturated solid solution and a structure formed by displacement of the eutectic point of Al-1.0 wt%Mn and Al-2.0 wt%Mn alloys, microphotographs at sections parallel and perpendicular to a chilled surface are shown in Photo. 5.

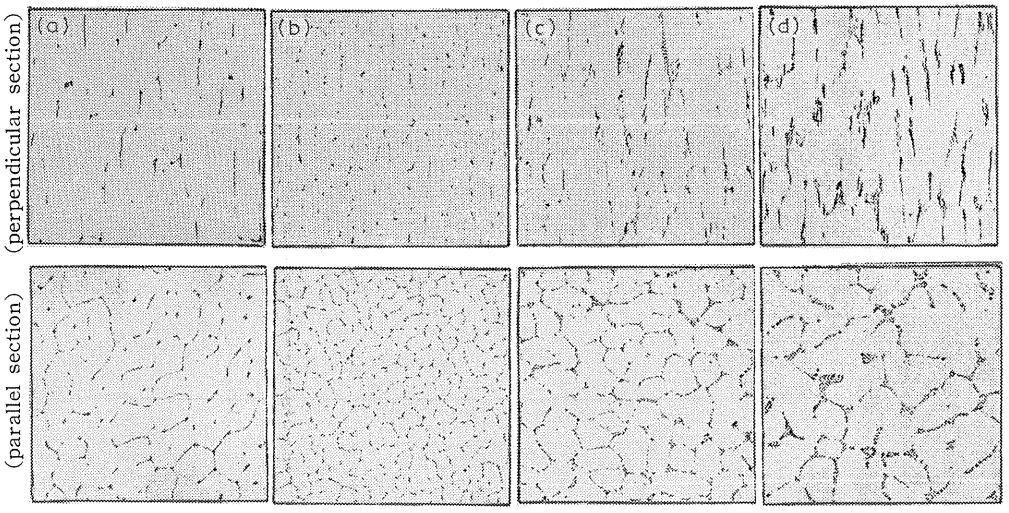

Photo. 5. Microstructures at sections, parallel and perpendicular to the chilled surface, of Al-Mn alloys. (X 150)
(a) 1.0 wt%Mn alloy,
(b) 2.0 wt%Mn alloy (completely super-saturated solid solution),
(c) 2.0 wt%Mn alloy (incompletely super-saturated solid solution),
(d) 2.0 wt%Mn alloy (structure formed by displacement of the eutectic point)

These show the structure morphology which are consisted of long-ellipsoid-like cells arranged in the direction of solidification as close-packed state. Also the structures of a completely super-saturated solid solution and an incompletely super-saturated solid solution of an Al-2.9 wt%Mn alloy are the same as those in Photo. 6. According to the microstructures shown in Photo. 5 and Photo. 6 and the results of thermal analysis, a solidification model would be assumed as follows, that is, solidification advanced by movement of the solid-liquid region in which columnar or rotated ellipsoid-like cells are arranged in front of a perfectly solidified layer as close-packed state. This is illustrated by Fig. 19 (a). This solidification mode is named as the exogenous mushy-cellular solidification. Within this solid-liquid region, the element of an equilateral hexagon (L is the length of one long side) on a perpendicular plane to the solidification direction is assumed and a local solidification model is as follows : (1) a solid phase is a collectivity of cells in which each has a circular section of radius r, (2) the solid phase increases its thickness with the progress of local solidification (Fig. 19 (b)) and (3) these cells are arranged in close-packed state in the solid-liquid region[48]. Therefore, when at

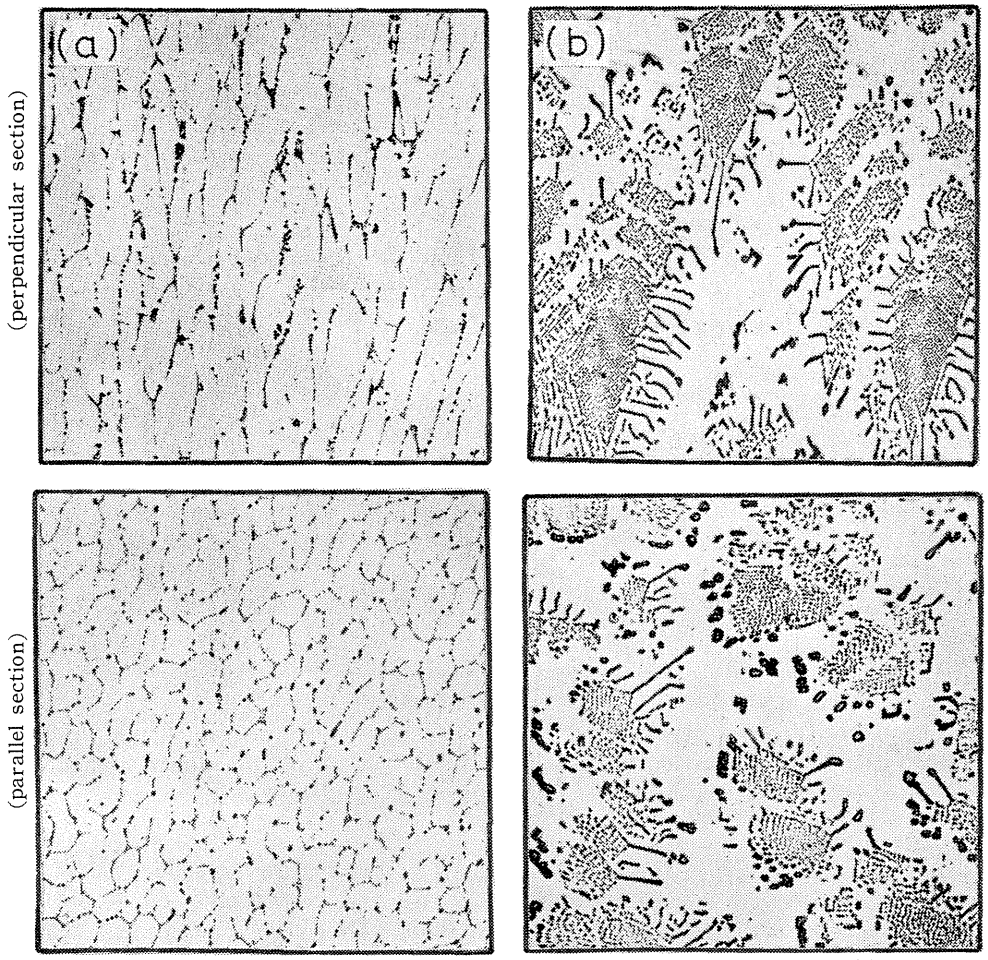

Photo. 6. Microstructures at sections, parallel and perpendicular to the chilled surface, of super-saturated Al-2.9 wt%Mn solid solutions. (X 300)
(a) completely super-saturated solid solution
(b) incompletely super-saturated solid solution of a cellular eutectic type

a certain thickness distance within the solid-liquid region average radius of cells is r, solid fraction f_s is given from Eq. (3):

$$f_s=(2\pi/\sqrt{3})\cdot(r^2/L^2) \tag{3}$$

In this case, it is assumed that average radius of cells (r) is in proportion to the square root of the elapsed time from the beginning point of local solidification (θ)[17]:

$$r=K\cdot\sqrt{\theta}\quad(0\leq r\leq L/2,\ K:\text{ constant}) \tag{4}$$

Using Eq. (4), the relation between cell spacing L and true local solidification time θ_f is Eq. (5):

$$L/2=K\cdot\sqrt{\theta_f} \tag{5}$$

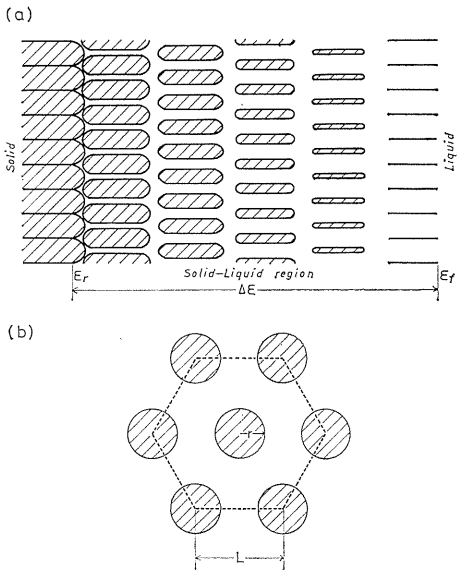

Fig.19. A rapid solidification model used for the analysis of solidification mode.

The true local solidification time θ_f is obtained by Eq. (6), using the local solidification time measured on a cooling curve Δt_i and the time taken when the front of a perfectly solidified layer (solid fraction $f_s=1$ within the solid-liquid region) passes through a hot junction $(t_p)_i$:

$$\theta_f=\Delta t_i-(t_p)_i \tag{6}$$

By substituting Eqs. (4), (5) and (6) into Eq. (3), the change of solid fraction at a thickness distance D_i within the solid-liquid region is expressed by Eq. (7), which is in proportion to the elapsed time of local solidification θ:

$$f_s(D_i,\ \theta)=A\cdot\theta\quad(A=\pi/[2\sqrt{3}(\Delta t_i-(t_p)_i]) \tag{7}$$

Subsequently, transforming the Eq. (3) that expresses solid fraction f_s at which the average radius of cells is r, the average radius r of cells during local solidification at a thickness distance D_i where solid fraction is f_s within the solid-liquid region is obtained by Eq. (8):

$$r(D_i,\ \theta)=0.525\cdot L\cdot\sqrt{f_s(D_i,\theta)} \tag{8}$$

The increasing rate of a cell radius (dr/dt) is obtained by Eq. (9):

$$dr/dt=0.263\cdot A\cdot L/\sqrt{f_s(D_i,\ \theta)} \tag{9}$$

5. 2. The solidification mode of super-saturated solid solutions

In the first place, the distribution of solid fraction within the solid-liquid region with the progress of solidification was calculated from Eq. (7) and on the basis of this result, the solidification mode of the case forming super-saturated solid solutions was examined. The change of $f_s(D,\ t_0)$ is shown in Fig. 20 (a) and (b) for

Al-2.0 wt%Mn and -2.9 wt%Mn alloys, respectively. Solid lines indicate the change in $f_s(D, t_0)$ of the case formed the completely super-saturated solid solutions and broken lines that of the case formed the incompletely super-saturated solid solutions. Furthermore, in the case of the completely super-saturated solid solutions the distribution is with $d^2f_s/dD^2<0$ (convex upward) while in the case of the incompletely super-saturated solid solutions with $d^2f_s/dD^2>0$ (convex downward). This fact manifests that in the case of the incompletely super-saturated solid solutions growing much, liquid phase exists as far as the deep points of the solid-liquid region and when cells thicken the occasion that the cell interface contacts with liquid phase is more than in the case of the completely super-saturated solid solutions.

When the distribution of solid fraction $f_s(D, t_0)$ described above changes by solidification progressing, the distribution on the average radiuses of cells, which are growing and thickening in the solid-liquid region, $r(D, t_0)$ is shown in Fig. 21. Fig. 21 (a) is for the case of an Al-2.0 wt%Mn alloy and Fig. 21 (b) for the case of an Al-2.9 wt%Mn alloy. The point plotted at the time $t_f(=t_1+\theta_f)$ in the case of the small thickness distance D_1 in the diagrams, (that is, a point at the left

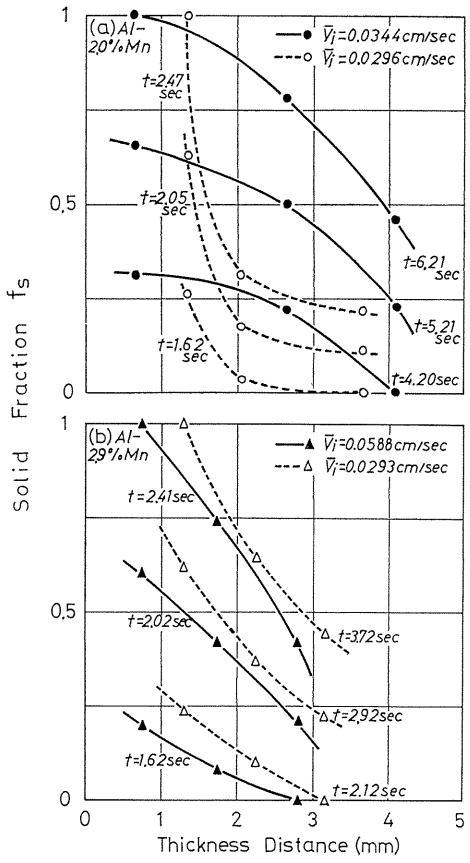

Fig. 20. Change of solid fraction with solidification progressing of super-saturated Al-Mn solid solutions.

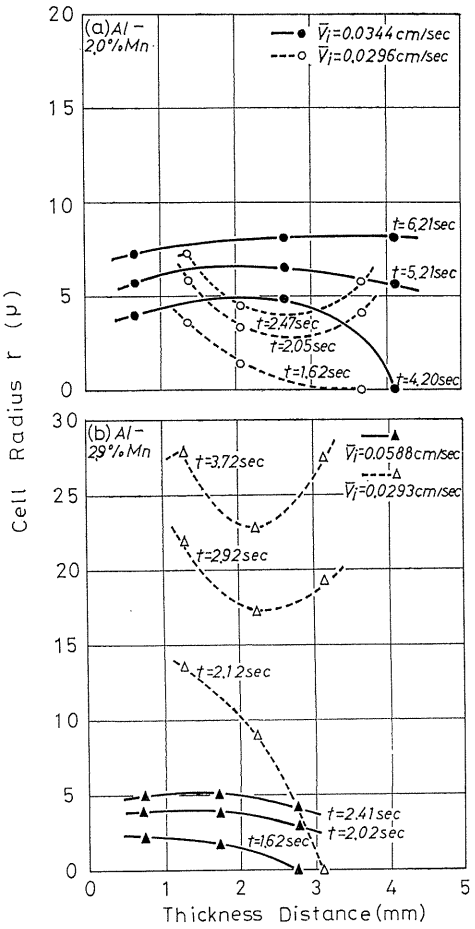

Fig. 21. Change of average radius of solid cells with solidification progressing of super-saturated Al-Mn solid solutions.

upper side) is the point corresponding to 1 in solid fraction f_s and r indicates the cell radius immediately after the completion of local solidification. The change in these distribution curves shows aspects of the distribution of the average radiuses and the thickening and growth of solid cells at the time when the solid-liquid region passes through from thickness distance D_1 to D_3 with time elapsing from t_3 to $(t_1+t_3+t_f)/2$ and $t_1+\theta_f$. Broken lines are the distribution curves for the case of the incompletely super-saturated solid solutions and solid lines are those for the case of the completely super-saturated solid solutions. Regarding the distribution on the average radius of solid cells a minimum value exists, as the thickening and growth of solid cells near the front of a perfectly solidified layer perhaps are slower than those of solid cells at far ahead.

5. 3. *The thickening rate of solid cells (local solidification process)*

Fig. 22 shows the thickening rate of the radiuses of solid cells with the progress of local solidification for super-saturated solid solutions of Al-2.0 wt%Mn and

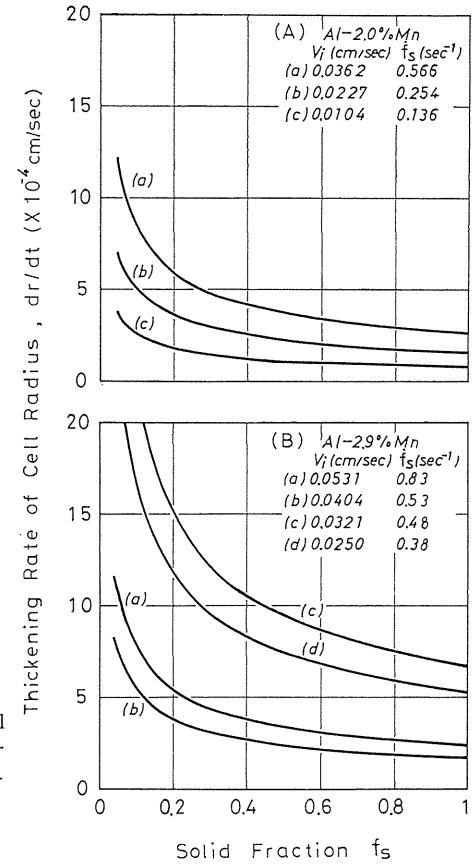

Fig. 22. Change in thickening rate of cell radius during local solidification for super-saturated Al-Mn solid solutions.

Al-2.9 wt%Mn alloys obtained by different solidification rates. Fig. 22 (A) is the case of an Al-2.0 wt%Mn alloy and the curve (a) shows the local solidification process of the completely super-saturated solid solution, (b) that of the incompletely super-saturated solid solution and (c) that of the structure formed by displacement of the eutectic point. In the case of an Al-2.9 wt%Mn alloy shown in Fig. 22 (B), the curve (a) shows the local solidification process of the completely super-saturated solid solution, (b) of the incompletely super-saturated solid solution of a hypo-eutectic type, (c) and (d) of the incompletely super-saturated solid solution of a cellular eutectic type. These thickening rates of the radiuses of solid cells (dr/dt) diminish with an decrease in solidification rates (V_i). Then, in the early stage of local solidification less than 0.1 in solid fraction (f_s), the thickening rate of the radiuses of solid cells is very fast and decreases steeply with the progress of local solidification. Next, in solid fractions more than 0.2, the thickening rates become the order of about 10^{-4} cm/sec.

5. 4. *The theoretical interpretation of the super-saturated solid solubility phenomenon*

The consideration on the super-saturated solid solubility phenomenon of Al-Mn alloys was tried on the basis of the thickening and growth rates of solid cells and

diffusion coefficient of manganese atoms in supercooled molten aluminium. In this experiment under the conditions of solidification rates from 0.5×10^{-2} to 7×10^{-2} cm/sec (cooling rates from 30 to 250 ℃/sec), since during local solidification time θ_f the solid-liquid region moved much larger than the diffusible distance of manganese atoms, the change of structures induced by the segregation of manganese atoms in the direction of solidification can not be considered. Therefore, in the consideration on the change of structures, it is necessary to compare the diffusion velocity of manganese atoms in the local solidification direction perpendicular to the direction of solidification with the thickening rate of solid cells. For Al-2.0 wt%Mn and Al-2.9 wt%Mn alloys, the changes in the amount of thickening of a solid cell during a very short time $\delta\theta$ with an increase in solidification rates V_i are shown in Fig. 23 by solid lines. Then, broken lines show maximum limits of

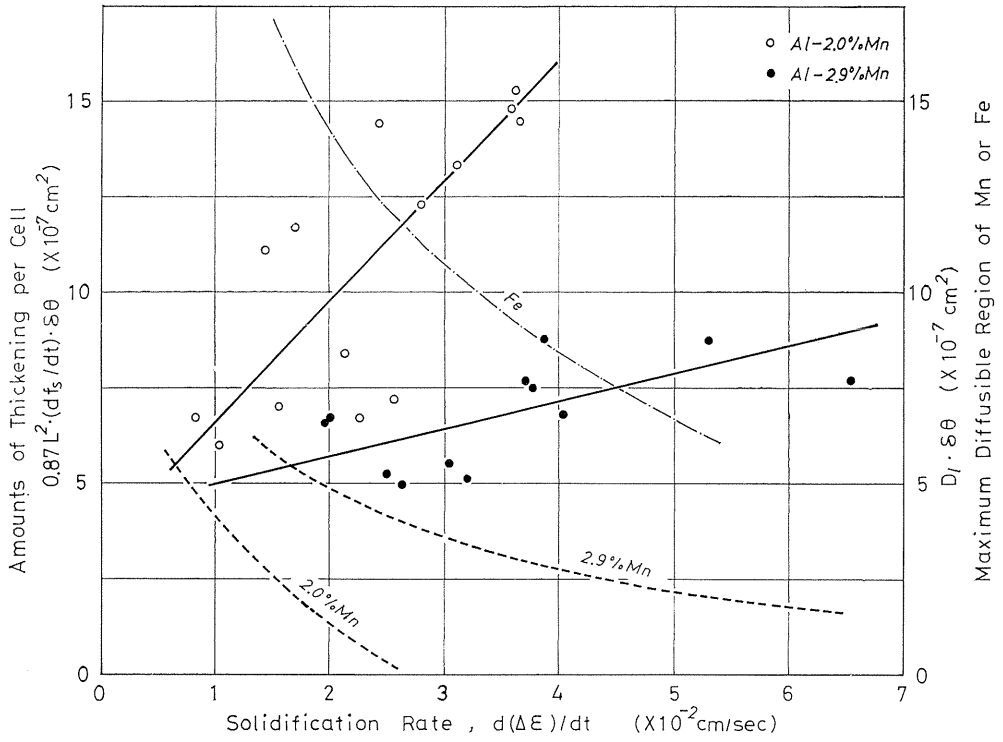

Fig. 23. Relation between the amounts of thickening per cell and the maximum diffusible region of manganese atom (or iron) for a very short time $\delta\theta$.

the diffusible region of manganese atoms in molten aluminium existing in the neighborhood of solid cell interface at a supercooling temperature during local solidification. In solidification rates over 0.7×10^{-2} cm/sec for an Al-2.0 wt%Mn alloy and over 1.8×10^{-2} cm/sec for an Al-2.9 wt%Mn alloy, the amount of thickening of a solid cell is larger than the maximum diffusible region, so that the condition in which the interface of solid cells traps manganese atoms, that is, the conditions for formation of a super-saturated solid solution are satisfied. These solidification

rates described above, agree almost with the minimum solidification rates required to form the super-saturated solid solution for each alloy. These minimum solidification rates were obtained from the changes in lattice parameters and hardness mentioned previously. Then, in spite of the solidification in the ranges of solidification rates to form completely super-saturated solid solutions for manganese, Al_6Fe compounds crystallized on cell boundaries. For explanation of this phenomenon, it must be considered that iron cannot dissolve in solid aluminium matrix in super-saturated state, that is, in Fig. 23 the solid lines showing the amount of thickening of a solid cell exist under a dotted chain line at these solidification rates.

6. The phase decomposition of a completely super-saturated solid solution[35]

6. 1. Isothermal heating

The heat treatment characteristics of a completely super-saturated Al-3.0 wt%Mn solid solution was investigated. Mechanical properties of the alloy were improved at such remarkably rapid solidification state (especially in toughness). Fig. 24 is the change showing the progress of age-hardening by isothermal heating

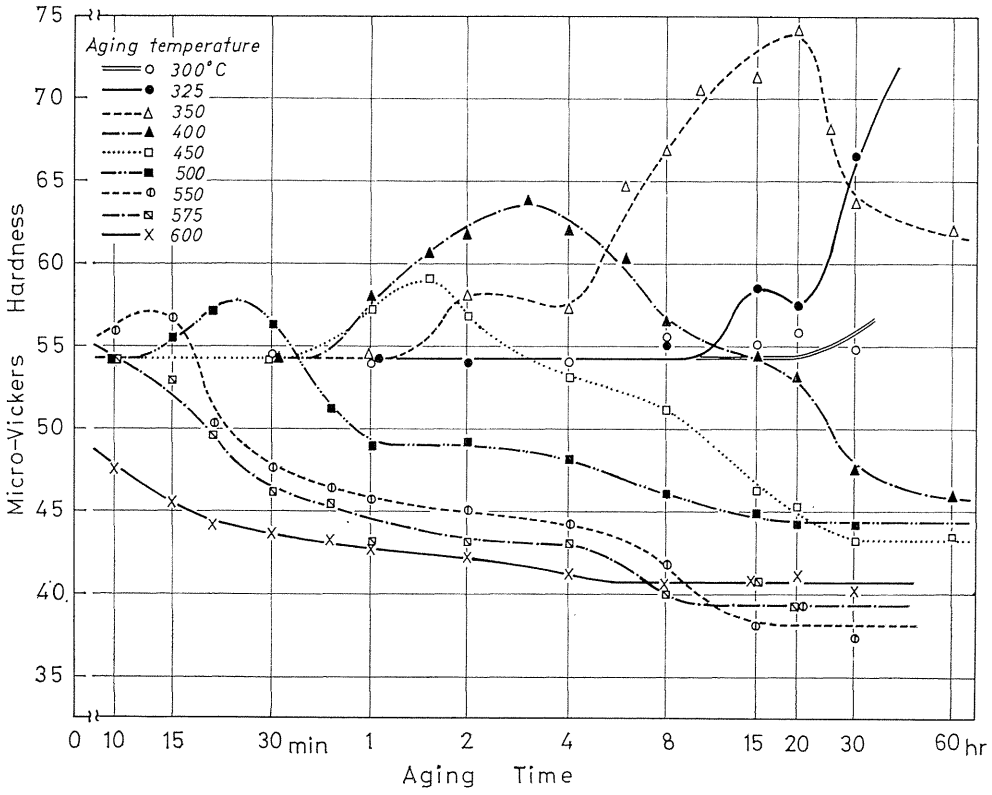

Fig. 24. Change in micro-Vickers hardness during isothermal heating in Al-3 wt%Mn super-saturated solid solution at various temperatures.

for the completely super-saturated solid solution. Even if heating temperature is 300℃, the super-saturated solid solution is considerably stable[49] and its hardening is not recognized. However, in the case heated for a long time at higher heating temperature, i. e. from 325℃ to 350℃, the alloy showed remarkable age-hardening and slightly softened after hardening. The hardening is based on precipitation of G-phase[50] and after precipitation - decomposition hardness values were kept at constant. When those constant values of some aging temperatures are compared each other, the values above 550℃ are lower than those below 550℃.

Next, Fig. 25 shows the change in lattice parameter with isothermal heating for the completely super-saturated solid solution. In the case of aging below 500℃, lattice parameter changed continuously and in the initial stage of precipitation - decomposition before reaching the maximum hardness, two values of lattice pa-

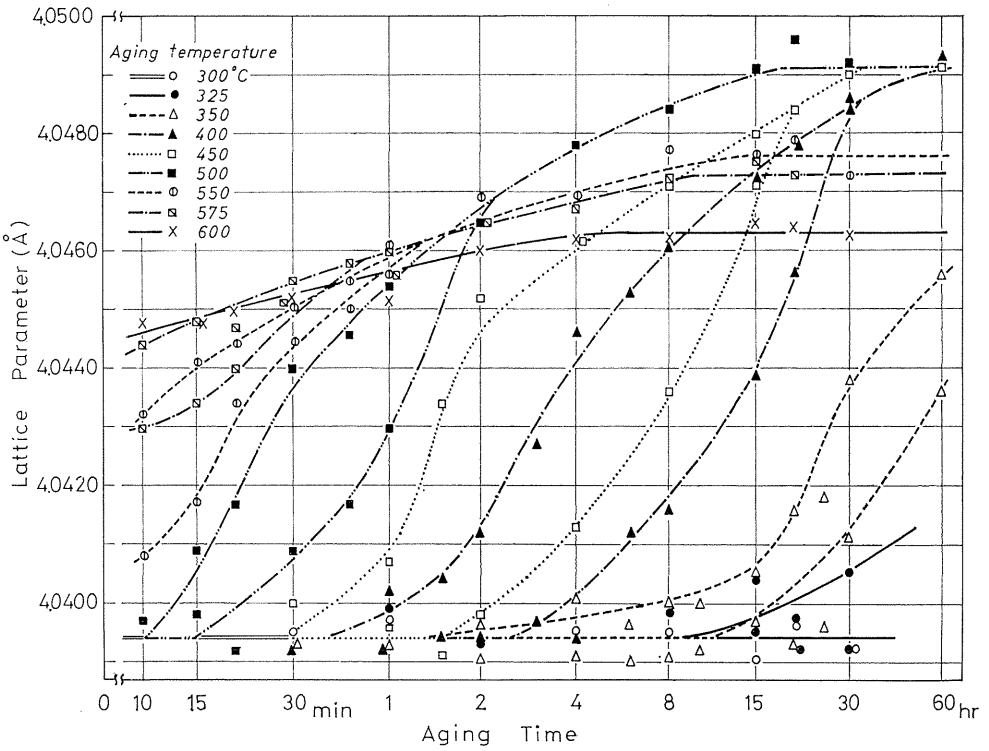

Fig. 25. Change of the lattice parameter during isothermal heating in Al-3 wt%Mn super-saturated solid solution at various temperatures.

rameter were measured,[51] that is, the one value corresponds to the completely super-saturated solid solution and the other to the region in which decomposition proceeded. In the middle stage of precipitation - decomposition, decomposition began in the undecomposed region and those two values of lattice parameter increased together according to a reaction formula of the first degree. After decomposition reached the last stage of precipitation - decomposition, the lattice parameter had again one value and approached to the value corresponding to the equilibrium state.

In case of 550℃ and 575℃ aging, after at 10 min heating the decomposition

began and its behavior was already similar to those of the middle stage of precipitation - decomposition at lower aging temperatures. At 600℃ aging, the separation of lattice parameter i. e. being of two lattice parameters, is not recognized and decomposition has already attained to the last stage of precipitation - decomposition.

6. 2. Precipitated phases and precipitation process

Fig. 26 is a diagram summarized the change and the species of precipitates with the decomposition of the super-saturated solid solution for aging temperatures

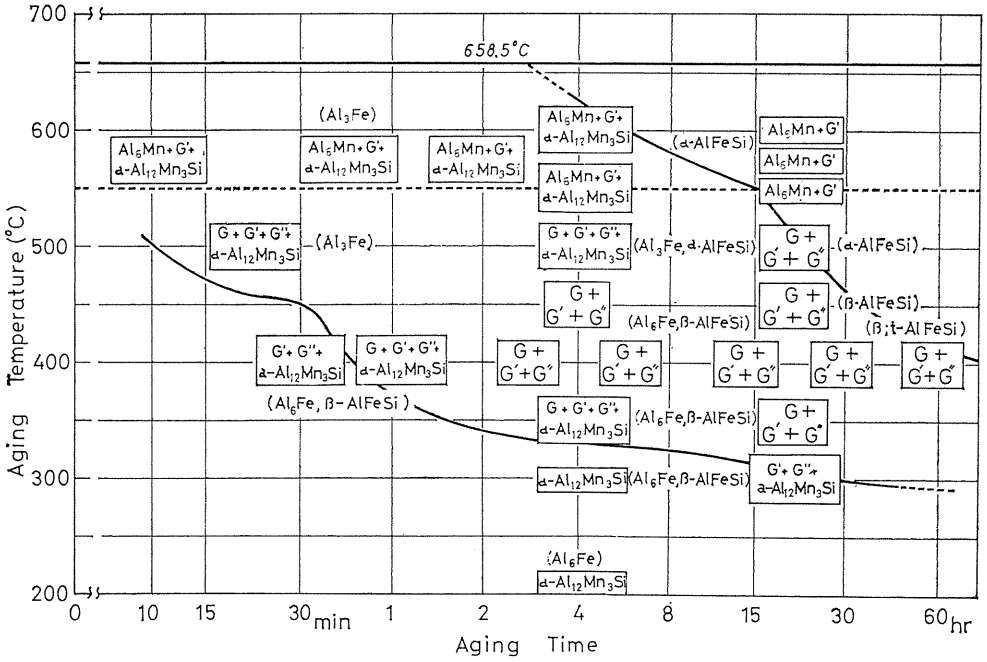

Fig. 26. Time-temperature-transformation diagram entered decomposition products of Al-3 wt%Mn super-saturated solid solution obtained by the heat treatments.
□ precipitated phase containing manganese
( ) precipitated phase formed by the impurity element

and time. At aging below 550℃ and in the quite early stage of decomposition when the change in lattice parameter begins, the G′-phase induced by impurities (simple cubic system, $a_0 = 12.75 \pm 0.15$ Å)[50, 52] and the metastable phase G″-phase (hexagonal system, $a_0 = 7.54 \pm 0.07$ Å, $c_0 = 7.84 \pm 0.08$ Å)[50, 53] are confirmed and in case decomposition proceeded further, the G-phase (b. c. c. system, $a_0 = 7.54 \pm 0.08$ Å)[50, 54] appears. In the middle stage of precipitation - decomposition, the relative amount of the G-phase increased with aging time. These three phases of the G-, G′- and G″-phases coexist, even after precipitation - decomposition finished. On the one hand, at heating temperatures above 550℃ the equilibrium phase Al_6Mn and the G′-phase were confirmed even in the initial stage of decomposition of 10

min at 575℃. Though at heating temperatures below 500℃ the precipitation - decomposition process is yet in the incubation period for the precipitates containing manganese, compounds containing impurities (iron and silicon) were already recognized as the Al_6Fe, β-Al-Fe-Si (monoclinic system, $a_0=b_0=6.12$Å, $c_0=41.48$Å, $\beta=91°$)[42] and α-$Al_{12}Mn_3Si$ by aging at this temperature range. In the initial stage of precipitation - decomposition, the α-$Al_{12}Mn_3Si$ disappeares to grow continuously into the G′-phase[50] and with the progress of precipitation - decomposition, the Al_6Fe decomposes and becomes the β-Al-Fe-Si.

At heating temperatures above 500℃, the Al_6Fe has already changed into the Al_3Fe in the incubation period and this Al_3Fe reacts on silicon which was isolated by the decomposition of the α-$Al_{12}Mn_3Si$ and consequently, precipitates as the α-Al-Fe-Si. Therefore, iron and silicon as impurity elements precipitate as binary Al-Fe compounds (Al_3Fe and Al_6Fe) and ternary compounds (α-$Al_{12}Mn_3Si$, α-Al-

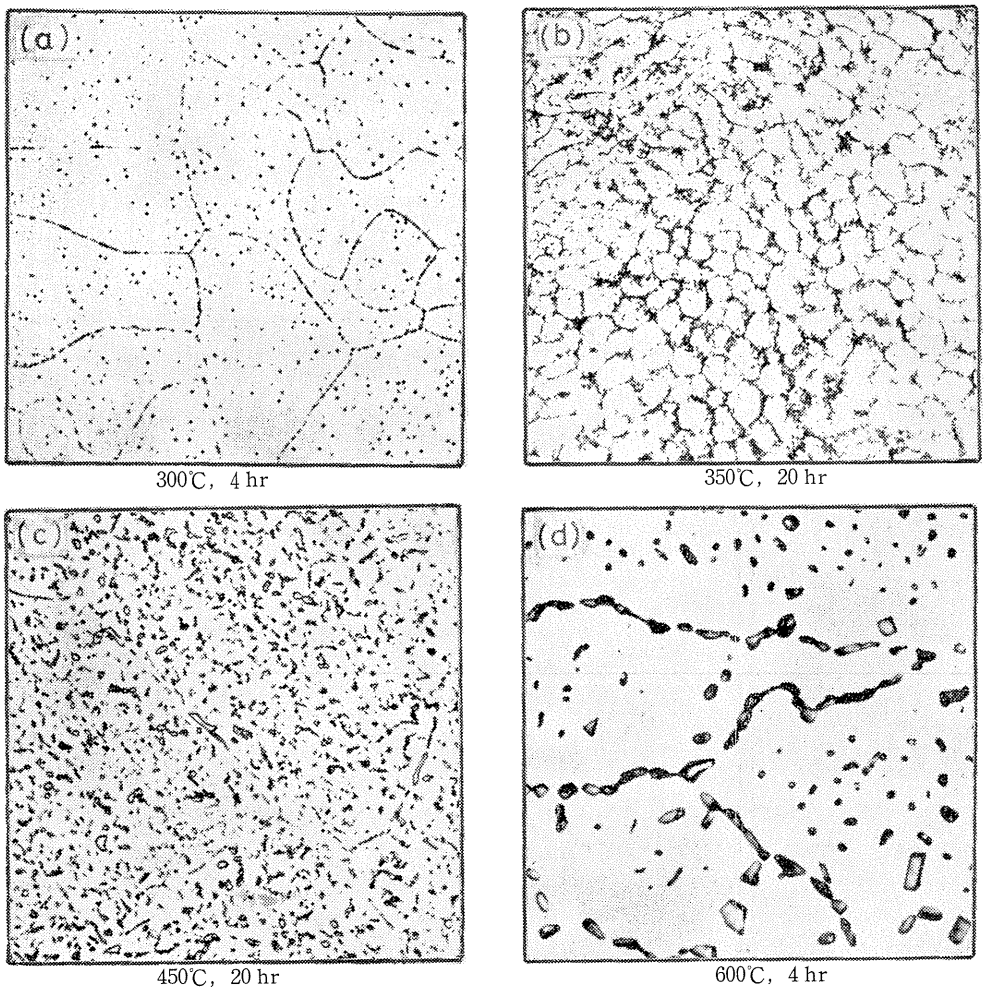

Photo. 7. Microstructures of Al-3 wt%Mn super-saturated solid solution heated for 4 and 20 hr at various temperatures. (X 800)

Fe-Si and β-Al-Fe-Si) and it can be understood by the decomposition reaction of those compounds that the iron and silicon have great influences upon the nucleation and growth rate of the precipitates containing manganese. Typical examples of the change in microstructures for the precipitation - decomposition of the super-saturated solid solution described above are shown Photo. 7. The structure of (a) is that in the incubation period for the precipitates containing manganese. However, the Al_6Fe and, the ternary compounds α-$Al_{12}Mn_3Si$ and β-Al-Fe-Si precipitate at cell and grain boundaries. The structure of (b) is that in the initial stage of precipitation - decomposition. The G-phase forms by nucleating any of G'-, G''-phases and the compounds containing the impurities and the hardness attains to the maximum value, and it became evident by micrograph observation that the precipitates grow along cell boundaries. The structure of (c) is that in last stage of precipitation - decomposition and precipitates have grown to cylindrical or acicular particles and also the precipitation in cell interior is recognized. The structure of (d) is that in a finished state of precipitation - decomposition at a heating temperature of 600℃. In the structure, the Al_6Mn, G'-phase and α-Al-Fe-Si coexist and Ostwald growth[55] of those precipitates can be observed. Namely it becomes evident that small precipitates at grain interior dissolve and the coasening of plate-like precipitates takes place on grain boundaries.

7. The analysis on the precipitation - decomposition process in a completely super-saturated solid solution[36]

7. 1. The analysis method of the precipitation - decomposition process

Fig. 27 is the schematic diagram showing the results which converted the values of the change in lattice parameter shown in Fig. 26 with isothermal heating

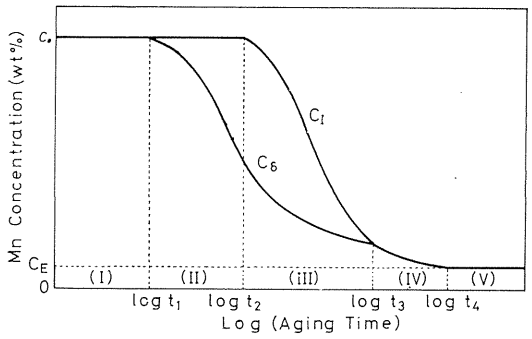

Fig. 27. Typical change of the manganese concentration in the super-saturated solid solution with aging time during isothermal heating.

into the manganese concentrations in the solid solution using the known relation[30] between manganese solid solubility and lattice parameter. This change in manganese concentration would be divided into five processes. The process (I) is the incubation period for the precipitation of phases containing manganese, the process (II) is the initial stage of the precipitation - decomposition, the process (III) is the middle stage, the process (IV) is the last stage and in the process (V) the precipi-

tation - decomposition process has completed. In the initial and middle stages, there are two values of lattice parameter at an aging time. This phenomenon perhaps must be caused by next two factors, i. e. (1) the diffusion velocity of manganese atoms is slow and (2) in addition precipitates nucleate and grow preferrentially at cell boundaries. The precipitation - decomposition processes (II) and (III) for this super-saturated Al-Mn solid solution are analyzed using a precipitation - decomposition model shown in Fig. 28.

The precipitation region has the cylindrical cell form connected each other with network. These are composed of the cell interior ($O \leq r \leq R_\delta$) with slight concentration gradient, the diffusion zone ($R_\delta \leq r \leq R_s$) and the precipitation zone ($R_s \leq r \leq L/2$), and this concentration profile is constructed by repeating the unit model in two dimensions. The concentration profiles shown in Fig. 29 are approximately expressed by Eq. (10) :

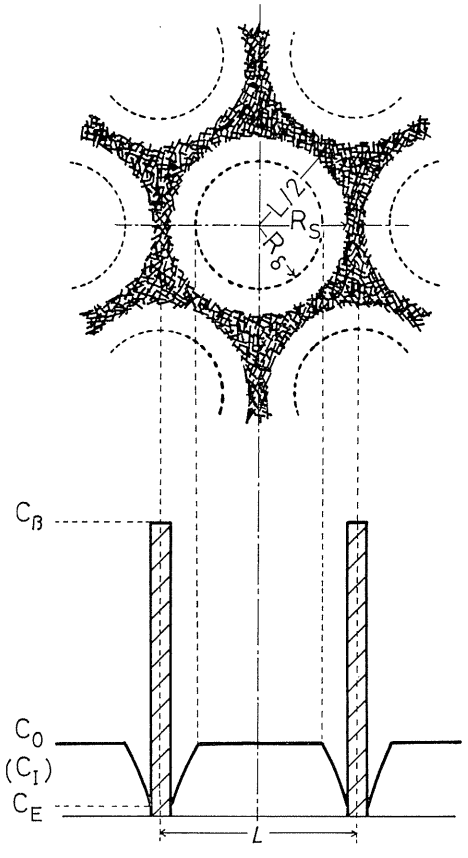

Fig. 28. The cylindrical cell model of precipitation based on the nucleation and growth mechanism.

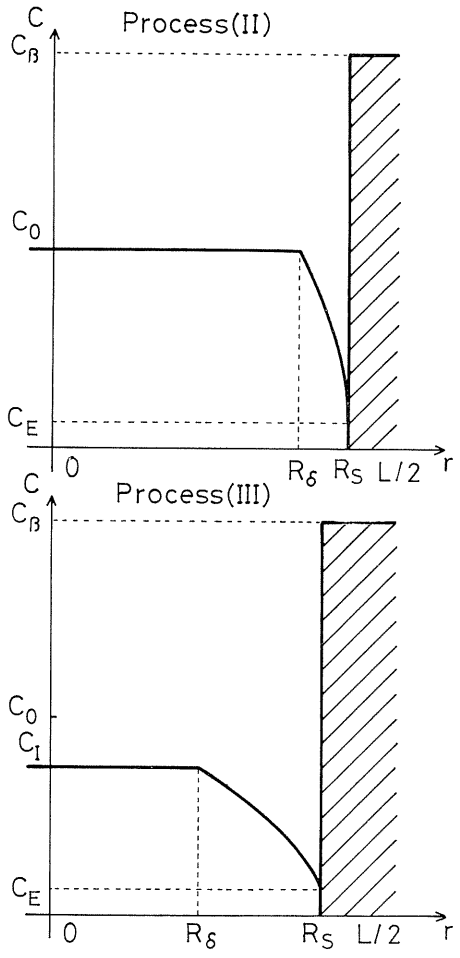

Fig. 29. Profiles on manganese concentration in a cylindrical cell hypothesized for the precipitation - decomposition processes (II) and (III).

$$\left.\begin{aligned} 0\leq r\leq R_\delta \quad &: C=C_I \\ R_\delta\leq r\leq R_s \quad &: C=(C_I-C_E)\cdot\sqrt[X]{(r-R_s)/(R_\delta-R_s)}+C_E \\ R_s\leq r\leq L/2 \quad &: C=C_\beta \end{aligned}\right\} \tag{10}$$

where X is the exponent which is determined according to heating temperatures. The C_I and C_δ are the manganese concentrations corresponding to diffraction lines from the cell interior and the diffusion zone respectively, and these were calculated from two values of lattice parameter determined for each heating time. An infinitesimal volume ΔV of range Δr with the very low concentration range ΔC $(=(C_I-C_E)/n$ i. e. the concentration profile in the diffusion zone are divided into n equal portions) is expressed as Eq. (11):

$$\Delta V=2\pi r\cdot|\Delta r|\cdot l \tag{11}$$

Therefore, the C_δ is expressed as Eq. (12) by i where ΔV has the maximum value:

$$C_\delta=\Delta C\cdot i_{max}+C_E \quad (\Delta V_{max}\longrightarrow i_{max}) \tag{12}$$

Furthermore, by substituting i_{max} into Eq. (12) and rearranging the results, the width ratio of the diffusion zone in matrix, R_δ/R_s is expressed as Eq. (13):

$$R_\delta/R_s=1-[(X-1)/(2X-1)]\cdot[(C_I-C_E)/(C_\delta-C_E)]^X \tag{13}$$

The boundary condition at the precipitation zone - diffusion zone interface is expressed by Eq. (14):

$$(C_\beta-C_E)\cdot(dR_s/dt)=D\cdot[(C_E-C_I)/(R_s-R_\delta)] \tag{14}$$

Differentiating y (precipitation fraction), which is ratio of the amount of manganese having precipitated at heating time t to initial manganese concentration in cell before heating, and substituting Eq. (13) and Eq. (14) further, the rates of precipitation dy/dt are expressed respectively for the initial process of precipitation - decomposition (II) by Eq. (15) and for the middle process of precipitation - decomposition (III) by Eq. (16):

$$t_1\leq t\leq t_2 \;:\; dy/dt=[(2X-1)/(X-1)]\cdot(8D/L^2)\cdot[(C_\delta-C_E)/(C_O-C_E)]^X \tag{15}$$

$$t_2\leq t\leq t_3 \;:\; dy/dt=[(2X-1)/(X-1)]\cdot(8D/L^2)\cdot[(C_\delta-C_E)^X/(C_I-C_E)^{X-1}\cdot(C_O-C_E)] \tag{16}$$

Precipitation fraction y becomes Eqs. (17) and (18) by integrating the rate of precipitation:

$$t_1\leq t\leq t_2 \;:\; y=[(2X-1)/(X-1)]\cdot(8D/L^2)\cdot[1/(C_O-C_E)^X]\cdot\int_{t_1}^{t}[C_\delta(t)-C_E]^X dt \tag{17}$$

$$t_2\leq t\leq t_3 \;:\; y=[(2X-1)/(X-1)]\cdot(8D/L^2)\cdot\{[1/(C_O-C_E)]\cdot\int_{t_2}^{t}[C_\delta(t)-C_E]^X/[C_I(t)-C_E]^{X-1}dt+[1/(C_O-C_E)^X]\cdot\int_{t_1}^{t_2}[C_\delta(t)-C_E]^X dt\} \tag{18}$$

The last process of precipitation - decomposition is expressed as Eq. (19)[56]:

$$t_3 \leq t \leq t_4 \ : \ y=[C_0-C_I(t)]/(C_0-C_E) \tag{19}$$

The values for exponent X in the equation described previously are confined to Eq. (20) and R_δ/R_s is from 0 to 1 and determined by integrating precipitation fraction y from t_1 to t_4 and in heating time 1.

$$X \geq 1, \ [(C_0-C_E)/(C_\delta-C_E)]^X \leq (2X-1)/(X-1) \tag{20}$$

7. 2. The kinetic consideration on the precipitation process

The Johnson - Mehl formula (Eq. (21))[57] was applied for the precipitation fraction y caluculated from the precipitation - decomposition model and the precipitation process of the super-saturated solid solution during isothermal heating was considered qualitatively.

$$y=1-exp[-(t/\tau)^m] \tag{21}$$

Fig. 30 is expressed those values by means of $\log[-\ln(1-y)]$ vs. $\log t$. The exponent m is the gradient of those straight lines and is the parameter expressing the nucleation and growth mechanism and the configuration of precipitates. At heating temperatures below 500℃, the initial process of precipitation, in which the G-phase nucleated after the G′- and G″-phases nucleated and grew to some extent, takes about 5/2 for the parameter m and the nucleation and the diffusion controlled growth takes place simultaneously.[58] Afterward, the middle process of precipita-

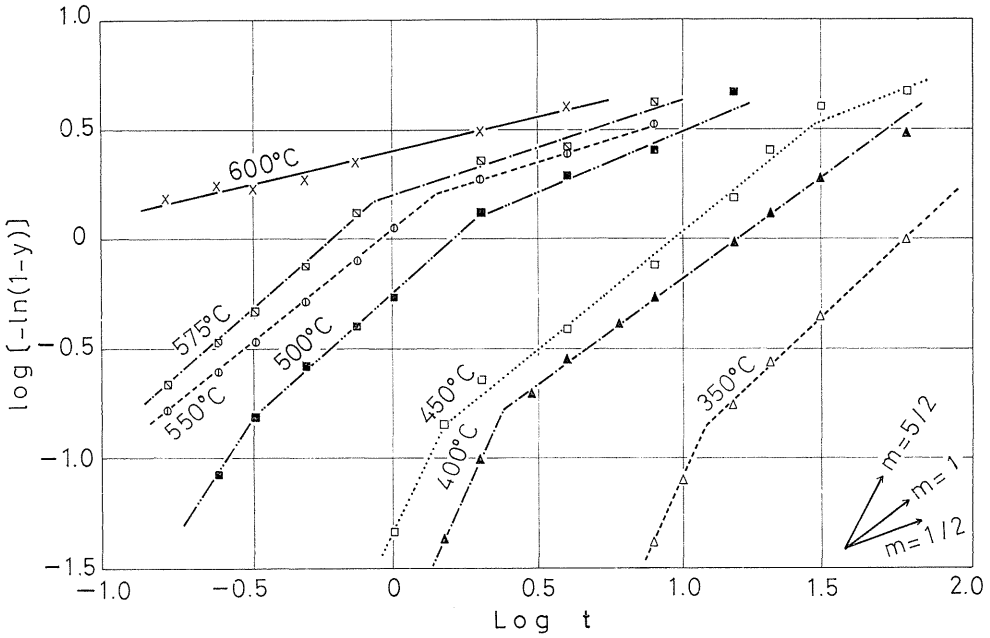

Fig. 30. Relation between precipitation fraction and aging time plotted on the basis of the Johnson-Mehl equation.

tion, in which fine acicular (cylindrical) or long and thin plate type precipitates were observed, takes about 1 for the parameter m and agrees with the process in which cylindrical precipitates are obtained by the diffusion controlled growth in the axial direction.[59] In the last process of precipitation, in which the nucleation in the cell interior and the growth of precipitates at the precipitation zone of cell boundaries begin again, the parameter m is converted into 1/2 and consequently this process can be interpreted as the process that precipitation takes place on dislocations in the cell interior.[53]

Then, at heating temperatures of 550℃ and 575℃, after 10 min isothermal heating the precipitation process was thought to be already at the end in the initial process or at the beginning in the middle process, therefore the figures showed the inclinations corresponded to the middle process of precipitation that the parameter m takes about 1 and then to the last process of precipitation that the parameter m takes about 1/2. However, at a heating temperature of 600℃ the precipitation process has proceeded sooner and even at 10 min heating is in the last process of precipitation and therefore the value of m is about 1/3 and it means that precipitates gather plate-like.[60]

7. 3. The decomposition process of a completely super-saturated solid solution

Fig. 31 is the schematic diagram of the decomposition process, that is, the super-saturated solid solution itself aged by the precipitation process described in the previous paragraph and the changes in concentration in cell matrix are estimated roughly from Eq. (13) and lattice parameter. The concentration profile (a) corresponds to the incubation period for precipitation of phases containing manganese, and those from (b) to (c) are that in the initial process of decomposition and decomposition preceeds rapidly at the diffusion zone. In the middle process of

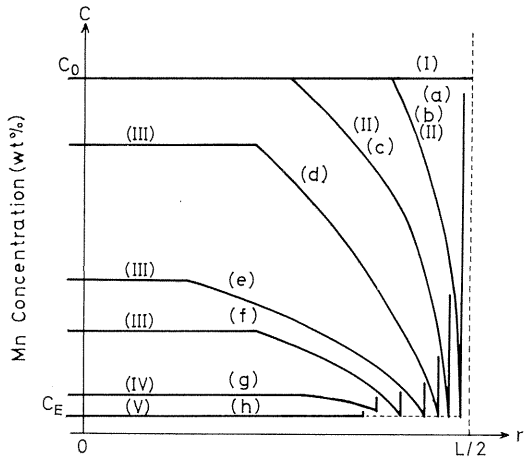

Fig. 31. Transition of schematic profiles of the manganese concentration in matrix with the decomposition of super-saturated solid solution.
(a) : $t \leq t_1$, (b) (c) : $t_1 \leq t \leq t_2$, (d) (e) (f) : $t_2 \leq t \leq t_3$,
(g) : $t_3 \leq t \leq t_4$, (h) : $t \geq t_4$

decomposition, from (d) to (e), decomposition proceeds even at the cell interior and is in the latter half of the middle process, from (e) to (f), the diffusion zone becomes narrow, since the diffusion of manganese atoms toward the diffusion zone decreases so that the concentration gradient in the diffusion zone may decrease. In the last process of decomposition, (g), the manganese concentration profile almost becomes uniform and a value close to the concentration of equilibrium solid solubility C_E. (h) indicates the profile after decomposition has finished.

7. 4. The activation energy for the precipitation - decomposition

Using the data on precipitation fraction y calculated from Eqs. (17), (18) and (19), the activation energy for precipitation - decomposition was calculated by means of the crosscut method. Consequently, in the case of heating temperatures below 550℃ at which the G-, G′- and G″-phases precipitated, the activation energy for precipitation was 21.4 kcal/mol and the activation energy of the Al_6Mn and G′-phase that precipitated at high temperatures above 550℃[61~64] was 40.7 kcal/mol. Also, the value obtained from heating times when the hardness attained to the maximum hardness for each heating temperature in isothermal heating was 23.7 kcal/mol below 550℃ and this value agreed nearly with the value obtained from the lattice parameter measurment described previously.

IV Summary

(1) When Al-Mn alloys are solidified by rapid cooling (about 50 to 300℃/sec in cooling rate), super-saturated solid solutions are formed comparatively easily. In this case, the thickness sensitivity is remarkable and especially, in Al-Mn alloys with hyper-eutectic compositions, the marked change of structure was found with variation in thickness distance. Those structures were classified as follows: i) the completely super-saturated solid solution of a single α-phase, ii) the incompletely super-saturated solid solution which is composed of the mixed structures of a super-saturated solid solution and secondary phases, iii) the primary compounds - eutectic structure corresponding to a structure formed by displacement of the eutectic point and iv) the primary compounds - α structure corresponding to an equilibrium structure. Furthermore, the species and changes of crystallized compound phases which composed those structures were elucidated.

(2) For Al-1.0 to 4.4 wt%Mn alloys, the distribution diagrams on the structures solidified by rapid cooling were obtained in regard to solidification rates and manganese contents.

(3) The mechanical properties of hyper-eutectic Al-Mn alloys were improved by controlled rapid cooling and especially, in the completely super-saturated solid solution of a single α-phase, the toughness value increased fairly.

(4) The conditions of the minimum solidification rates which is required to form super-saturated solid solutions were made clear. Furthermore, the interpretation on the solidification mode of super-saturated solid solutions and the super-saturated solid solubility phenomenon was proposed.

(5) When the completely super-saturated Al-3 wt%Mn solid solution of a high manganese composition was heated at heating temperatures from 325℃ to 350℃ isothermally, age-hardening took place fairly and the species and change of pre-

cipitated phases with its decomposition by heating were determined clearly.

(6) On the basis of the change in lattice parameter with the decomposition by heating of the completely super-saturated solid solution, the precipitation - decomposition process was made clear by analyzing and presented a precipitation - decomposition model in this case.

References

1) S. Nishi: B. Japan Inst. Metals, **11** (1970), 693.
2) E. L. Glasson and E. F. Emley: *The Solidification of Metals*, The Iron & Steel Institute, London, (1968), p. 1.
3) S. N. Singh and M. C. Flemings: Trans. Met. Soc. AIME, **245** (1969), 1811.
4) I. Maxwell and A. Hellawell: Met. Trans., **3** (1972), 1487.
5) W. C. Rotsell: *Light Metals 1972*, AIME, (1972).
6) S. Nishi: *The Refinement of Ingot Structure and the Problem with It*, Symposium of Japan Institute of Light Metals, (1973), p. 1.
7) H. D. Brody and M. C. Flemings: Trans. Met. Soc. AIME, **236** (1966), 615.
8) T. F. Bower, H. D. Brody and M. C. Flemings: Trans. Met. Soc. AIME, **236** (1966), 624.
9) M. C. Flemings and G. E. Nereo: Trans. Met. Soc. AIME, **239** (1967), 1449.
10) M. C. Flemings, R. Mehrabian and G. E. Nereo: Trans. Met. Soc. AIME, **242** (1968), 41.
11) R. Mehrabian, M. Keane and M. C. Flemings: Met. Trans., **1** (1970), 1209.
12) H. Matyja, B. C. Giessen and N. J. Grant: J. Inst. Metals, **96** (1968), 30.
13) M. Moss and D. H. Schuster: Trans. ASM, **62** (1969), 201.
14) M. H. Burden and H. Jones: J. Inst. Metals, **98** (1970), 249.
15) H. Ahlborn and D. Merz: Aluminium, **47** (1971), 671.
16) I. Obinata, E. Hata and K. Yamaji: J. Japan Inst. Metals, **17** (1953), 496.
17) T. Toda and R. Maddin: Trans. Met. Soc. AIME, **245** (1969), 1045.
18) C. P. Hinesley and J. G. Morris: Met. Trans., **1** (1970), 1476.
19) A. Tonejc, D. Rožák and A. Bonefačić: Acta Met., **19** (1971), 311.
20) T. Ikeda and S. Nishi: J. Japan Inst. Metals, **39** (1975), 147.
21) R. Ichikawa and T. Ohashi: J. Light Metals, **18** (1968), 314.
22) P. Predecki, A. W. Mullendore and N. J. Grant: Trans. Met. Soc. AIME, **233** (1965), 1581.
23) M. Moss: Acta Met., **16** (1968), 321.
24) D. R. Harbur, J. W. Anderson and W. J. Maraman: Trans. Met. Soc. AIME, **245** (1969), 1055.
25) E. Babić, E. Girt, R. Krsnik and B. Leontić: Journal of Physics E., **3** (1970), 1014.
26) S. Nishi and T. Ikeda: Report of Committee for the Promotion of Aluminium - Science and Technology, Liquid - Solidification Group, (1972), 14.
27) The Japan Institute of Metals: *Nonferrous Material* II, The Section of a Newly Published Material, (1965), p. 174.
28) S. Ishida: *Nonferrous Metals and the Alloys* (II), An Outline of Applied Metallurgy Vol. 8, Seibundo, (1964), p. 36.
29) S. Nishi: *Aluminium*, Whole Set of Inorganic Chemistry X-1-1, Maruzen, (1975), 348.
30) G. Falkenhagen und W. Hofmann: Z. Metallk., **43** (1952), 69.
31) P. Furrer und H. Warlimont: Z. Metallk., **62** (1971), 100.
32) T. Ikeda, S. Taga and S. Nishi: J. Japan Inst. Metals, **38** (1974), 462.
33) T. Ikeda, S. Nishi and H. Seo: J. Japan Inst. Metals, **40** (1976), 584.
34) S. Nishi and T. Ikeda: Report of Committee for the Promotion of Aluminium - Science and Technology, Liquid - Solidification Group, (1973), 1.
35) T. Ikeda and S. Nishi: J. Japan Inst. Metals, **40** (1976), 571.

36) T. Ikeda and S. Nishi: J. Japan Inst. Metals, **40** (1976), 578.
37) I. Nitsuta: *X-ray Crystallography*, The Last Volume, Maruzen, (1961), p. 57.
38) I. Obinata, D. Oelschlägel and Y. Takeuchi: J. Inst. Metals, **95** (1967), 158.
39) M. Hansen: *Constitution of Binary Alloys*, McGraw-Hill Book Company, 2nd., (1958), p. 110.
40) W. B. Pearson: *A Handbook of Lattice Spacings and Structure of Metals and Alloys*, Pergamon Press, London, (1958), p. 373.
41) A. D. Nicol: Acta Cryst., **6** (1953), 285.
42) G. Phragmén: J. Inst. Metals, **77** (1950), 489.
43) E. H. Hollingsworth, G. R. Frank, Jr. and R. E. Willett: Trans. Met. Soc. AIME, **224** (1962), 188.
44) P. J. Black: Acta Cryst., 8 (1955), 175.
45) A. Nagata, D. Oelschlägel, Y. Takeuchi and I. Obinata: Trans. JIM, **10** (1969), 52.
46) J. G. Fisher et al.: *Dislocations and Mechanical Properties of Crystals*, John Wiley & Sons, New York, (1957), p. 355.
47) H. Warlimont: Z. Metallk., **63** (1972), 113.
48) P. K. Rohatgi and C. M. Adams: Trans. Met. Soc. AIME, **239** (1967), 1737.
49) L. M. Burov and N. I. Varich: Phys. Met. Metallog., **16**, 4 (1963), 33.
50) E. Nes, S. E. Naess and R. Hoier: Z. Metallk., **63** (1972), 248.
51) Y. Murakami and K. Mori: J. Light Metals, **18** (1968), 339.
52) K. Little, G. V. Raynor and W. Hume-Rothery: J. Inst. Metals, **73** (1946), 83.
53) D. Oelschlägel, O. Kawano and O. Izumi: J. Light Metals, **20** (1970), 531.
54) G. Marchand: J. Inst. Metals, **73** (1946), 747.
55) R. A. Oriani: Acta Met., **12** (1964), 1399.
56) The Japan Institute of Metals: *Aging Process of Alloys and Its Interpretation*, (1968), p. 15.
57) W. A. Johnson and P. F. Mehl: Trans. Met. Soc. AIME, **135** (1939), 416.
58) J. Burke: Phil. Mag., **6** (1961), 1439.
59) F. S. Ham: J. Appl. Phys., **30** (1959), 1518.
60) Y. Murakami: *Introduction to Phase Transformations in Condensed System - Its Thermodynamics and Kinetics* -, Maruzen, (1968), 62.
61) D. B. Goel, P. Furrer und H. Warlimont: Aluminium, **50** (1974), 511.
62) J. J. Théler und P. Furrer: Aluminium, **50** (1974), 467.
63) L. M. Burov: Phys. Met. Metallog., **22**, 1 (1966), 128.
64) M. Moss and M. M. Karnowsky: Bull. Am. Phys. Soc., **14**, 11 (1969), 834.